Critical properties of $2D$ $Z(N)$ vector models for $N > 4$

Gennaro Cortese

Dipartimento di Fisica

Universitá della Calabria

A thesis submitted for the degree of

PhD in Fisica e Tecnologie Quantistiche

2011 November

1. Reviewer: Alessandro Papa

Day of the defense: 19 December

Signature from head of PhD committee:

Al piccolo Ambrogio De Marco

Non ti abbiamo dimenticato

ti teniamo stretto nel cuore

Anche se non sei piú qui con noi

il tuo spirito e il tuo sorriso

riempiono la nostra esistenza

Ti voglio bene Ambró

Acknowledgements

Voglio ringraziare innanzitutto il mio relatore Alessandro che ha reso possibile, tramite il suo aiuto e appoggio, il raggiungimento di questo obiettivo. Oltre ad essere stato per me una guida "scientifica" lo considero un vero e proprio amico.

Un grazie di cuore anche all' amico Mario Gravina, la cui collaborazione é stata fondamentale alla stesura del seguente lavoro e le sue discussioni sempre molto stimolanti sia che si parlasse di fisica che di altro.

Un grande ringraziamento anche a Oleg Borisenko per la sua preziosa e fruttuosa collaborazione e a Roberto Fiore per i suoi consigli e discussioni.

Per ultimo, voglio ringraziare mia madre, mio padre e naturalmente mia sorella Aida per il loro appoggio incondizionato e costante. Un saluto alla mia cara nonna Maria che se ne andata in un caldo giorno d'estate di un anno fa lasciandoci il ricordo di una vita orgogliosa di lavoro e sacrificio.

Contents

1

Introduction

The Berezinskii-Kosterlitz-Thouless (BKT) phase transition is known to take place in a variety of two-dimensional ($2D$) systems: certain spin models, two-dimensional Coulomb gas, sine-Gordon model, Solid-on-Solid model, etc., the most popular and elaborated case being the two-dimensional XY model (1, 2, 3). There are several indications that this type of phase transition is not a rare phenomenon in gauge models at finite temperature: one can argue that in some three-dimensional lattice gauge models the deconfinement phase transition is of BKT type as well. Here we are going to study an example of lattice spin model where this type of transition exhibits itself, namely the $2D$ $Z(N)$ spin model, also known as vector Potts model.

We first investigate the case $N = 5$, the lowest number where the BKT transition is expected. The motivation of our study is three-fold:

1. to compute critical indices at the transition points, which could serve as checking point of universality;

2. to shed light on the discrepancy in the literature concerning the $Z(5)$ model;

3. to develop and test a new version of Monte Carlo cluster algorithm valid for odd values of N.

The first motivation is related to the study of the finite-temperature transitions in $3D$ $Z(N)$ and $SU(N)$ lattice gauge theory (LGT). It is expected that in

1. INTRODUCTION

$3D$ $Z(N)$ LGT a deconfinement phase transition takes place at finite temperature. There is no precise statement about the order of the phase transition, but presumably it is of the BKT type if $N > 4$. If it is the case, the Svetitsky-Yaffe conjecture (12) implies that the $3D$ $Z(N)$ LGT is in the universality class of $2D$ vector Potts model.

Therefore, our investigation here can be viewed as a preliminary step in studying deconfinement phase transition in $3D$ $Z(N)$ and also in $SU(N)$ LGTs.

The second motivation reflects the fact that many features of the critical behavior of the $Z(5)$ model are not reliably established. Moreover, there are certain discrepancies even in determining the nature of the phase transition, *i.e.* whether the phase transition is of BKT type or not.

We briefly summarize the present state of arts.

- The rigorous proof of the massless phase existence in $2D$ $Z(N)$ models utilizes methods which do not allow to establish the exact value of N above which the BKT phase transition exists (10).

- Reliable analytical calculations can only be performed with the Villain formulation (that we define after); the RG study of Ref. (5) predicts that the massless phase exists for all $N > 4$.

- Though these models have an interesting but hard to uncover duality properties (15) some information on the phase structure of the general $Z(N)$ spin models can be obtained (see, e.g. (13)). These transformations cannot be used to establish the position of critical points in $Z(5)$ model (14). Nevertheless, one can predict an approximate phase diagram and argue that the massless phase and the BKT transition exist for $N = 5$ in a certain region of the parameter space (15, 16).

  For completeness we mention that in Refs. (17) it was suggested that there is only one first order phase transition in $Z(5)$ model.

- Monte Carlo simulations of the $Z(N)$ model have been performed in Refs. (11, 18, 19, 20). Results of Ref. (18), though obtained on rather small lattices, indicate that the BKT transition takes place in models with $N \geq 8$. This

contradicts the results of (11, 20) which well agree with the BKT behavior for $N = 6$.

However, most recent simulations of the helicity modulus (that we will introduce later) in the $Z(5)$ model at $\beta_c^{(1)}$ do not agree with what is expected at the BKT transition (19).

Still, it remains unclear how this behavior of the helicity modulus influences other features of the BKT transition.

The paper is organized as follows: in the first Chapter, after an introduction on the characteristic features of the BKT phase transition, we give a look at the $2D$ XY model, where the BKT phase transition is known to takes place and we introduced the $2D$ $Z(N)$ vector models. In the third Chapter we give an overview on the observables used and on the related quantities. In the fourth Chapter we illustrate the algorithm used for the Monte-Carlo simulations. The Chapter number five contains the results of the work and finally in the last Chapter there are some general discussions and future perspectives.

2

The Berezinskii-Kosterlitz-Thouless phase transition

Kosterlitz and Thouless (3) gave an intuitive and beautiful description of the phase transition in the planar (XY) model more than four decades ago. The transition separates a low temperature phase dominated by spin waves with the occasional appearance of bound vortex-antivortex pairs and a high temperature phase dominated by a gas of free vortices and antivortices that start to disorder the system resulting in a finite correlation length ξ. The correlation length of the BKT model in the neighbourhood of the transition temperature T_{BKT} behaves as

$$\xi \simeq \exp(b/t^{1/2}) \tag{2.1}$$

where $t = (T - T_{BKT})/T_{BKT}$ is the reduced temperature. It is conceivable that as T approaches T_{BKT} from above, the correlation length becomes larger than any moderate size lattices used for Monte Carlo simulations, before one reaches the asymptotic scaling region. Then of course any comparison with theoretical predictions becomes more fortuitous due to the presence of large finite size corrections. This means that only in the early nineties, Monte Carlo numerical methods allowed to favour the BKT behavior 2.1 over a power law characteristic for a second order phase transition expressed by $\xi \propto t^{-\nu}$.

2.1 The XY model: BKT transition at work

Since many years ago the $2D$ XY model has been extensively studied due to its interesting phase transition properties. It is well known that the $2D$ XY model, also known as planar rotator or planar $O(2)$ display a BKT transition at a finite temperature $T^{(2)}_{BKT} > 0$. A general way to write the partition function is the following

$$Z_{XY}[K_\mu, h] = \sum_{\{\theta_r\}} \exp\left[\sum_r \left(\sum_{\mu=1,2} K_\mu \cos\left(\theta_{r+e_\mu} - \theta_r\right) + h\cos\theta_r\right)\right], \qquad (2.2)$$

where the continuos angle variable θ_r take values in the interval $\theta_r = \theta_{i,j} \in [0, 2\pi)$ and $\cos\left(\theta_{r+e_\mu} - \theta_r\right)$ clearly represent the scalar product of two-component spins located at the vertices of a square lattice. The coupling $K_\mu = \beta J_\mu$ is the product of the inverse temperature $\beta = 1/k_B T$ and the coupling strength J_μ while the quantity h represent the temperature-rescaled external magnetic field that we set equal to zero in this case.

The XY model is governed by a (global) continuos $U(1)$ symmetry, meaning that the system is invariant under a simultaneous rotation of every spin in the lattice by the same angle. The *Mermin-Wagner theorem* states that the $2D$ XY model does not display spontaneous magnetization at finite temperature. Since a phase transition is said to takes place whenever a thermodynamic function of the system under study display a non-analiticity, the latter, in the case of the $2D$ XY model may occur even when the ground state is unique, in order that there is no spontaneous symmetry breakdown. The BKT transition at a finite and non-zero temperature $T^{(2)}_{BKT}$ is characterized by an essential singularity in the free energy and correlation length. In the region $T > T^{(2)}_{BKT}$, the correlators of the XY model decay exponentially with distance, as it happens in a typical disordered, paramagnetic phase. On the other hand, in the low-temperature region, $T < T^{(2)}_{BKT}$, the correlators decay algebraically with distance. The feature that this power-law behavior extends over the finite temperature range $0 < T < T^{(2)}_{BKT}$, without long-range order, is known as *quasi-long-range order*.

2.2 From the XY to $Z(N)$ vector models

The $Z(N)$ vector models represents an approximation of the XY model and a useful test ground for understanding the rich critical behavior characterizing these systems.

We consider a $2D$ lattice $\Lambda = L^2$ with linear extension L and we impose periodic boundary conditions on spin fields in both directions. The partition function of the model can be written as

$$Z(\Lambda, \beta) = \left[\prod_{x\in\Lambda} \frac{1}{N} \sum_{s(x)=0}^{N-1}\right] \left[\prod_{x\in\Lambda} \prod_{n=1,2} Q\left(s(x) - s(x+e_n)\right)\right] . \tag{2.3}$$

In the standard formulation the most general $Z(N)$-invariant Boltzmann weight with $N-1$ different couplings is

$$Q(s) \;=\; \exp\left[\sum_{k=1}^{N-1} \beta_k \cos\frac{2\pi k}{N} s\right] . \tag{2.4}$$

In the Villain formulation the Boltzmann weight reads instead

$$Q(s) \;=\; \sum_{m=-\infty}^{\infty} \exp\left[-\frac{1}{2}\beta\left(\frac{2\pi}{N}s + 2\pi m\right)^2\right] . \tag{2.5}$$

We can see that, in appearance, with the general $Z(N)$-invariant Boltzmann weight 2.4, this models are identical to the classical XY model (with the external magnetic field set to zero), except for the fact that now, the degrees of freedom are discrete and countable. However, in the large N limit ($N \to \infty$), we recover the XY model. The key feature of the massless BKT phase in $Z(N)$ models is then the enhancement of the discrete symmetry of the Hamiltonian: the symmetry of the ground state in the intermediate phase is rather $U(1)$ than $Z(N)$ (10). This can be observed in a characteristic distribution of the complex magnetization, in the power-like decay of the correlation functions in the massless phase, in the vanishing of the beta-function, etc.

Some details of the critical behavior of $2D$ $Z(N)$ spin models are well known – see the review in Ref. (4). The $Z(N)$ spin model in the Villain formulation (2.5) has been studied analytically in Refs. (5, 6, 7, 8, 9). It was shown that the model

has at least two phase transitions when $N \geq 5$. The intermediate phase is a massless phase with power-like decay of the correlation function. The critical index η has been estimated both from the renormalization group (RG) approach of the Kosterlitz-Thouless type and from the weak-coupling series for the susceptibility. It turns out that $\eta(\beta_{\rm c}^{(1)}) = 1/4$ at the transition point from the strong coupling (high-temperature) phase to the massless phase, *i.e.* the behavior is similar to that of the XY model. At the transition point $\beta_{\rm c}^{(2)}$ from the massless phase to the ordered low-temperature phase one has $\eta(\beta_{\rm c}^{(2)}) = 4/N^2$. A rigorous proof that the BKT phase transition does take place, and so that the massless phase exists, has been constructed in Ref. (10) for both Villain and standard formulations (with one non-vanishing coupling β_1). Monte Carlo simulations of the standard version with $N = 6, 8, 12$ were performed in Ref. (11). Results for the critical index η agree well with the analytical predictions obtained from the Villain formulation of the model.

3

Observables and quantities related

In this chapter I want to summarize the definitions of the observables that we have measured in our numerical simulations. Then we also show other quantities related to these.

3.1 The observables

Since we expect that the $2D$ $Z(N)$ vector models with $N > 4$ exhibit three different phase, clearly we need some useful quantities in order to characterize the two phase transitions.

The complex magnetization is given by

$$M_L = \frac{1}{L^2} \sum_i \exp\left(i \frac{2\pi}{N} s_i\right) \equiv |M_L| e^{i\psi} \ . \tag{3.1}$$

In Fig. **??** we show the scatter plot of M_L on a lattice with $L = 64$ in $Z(5)$ at three values of β, each representative of a different phase: $\beta = 0.80$ (high-temperature, disordered phase), $\beta = 1.10$ (BKT massless phase) and $\beta = 1.50$ (low-temperature, ordered phase). As we can see we pass from a uniform distribution (low β) to a ring distribution (intermediate β) and finally to five isolated spots (high β).

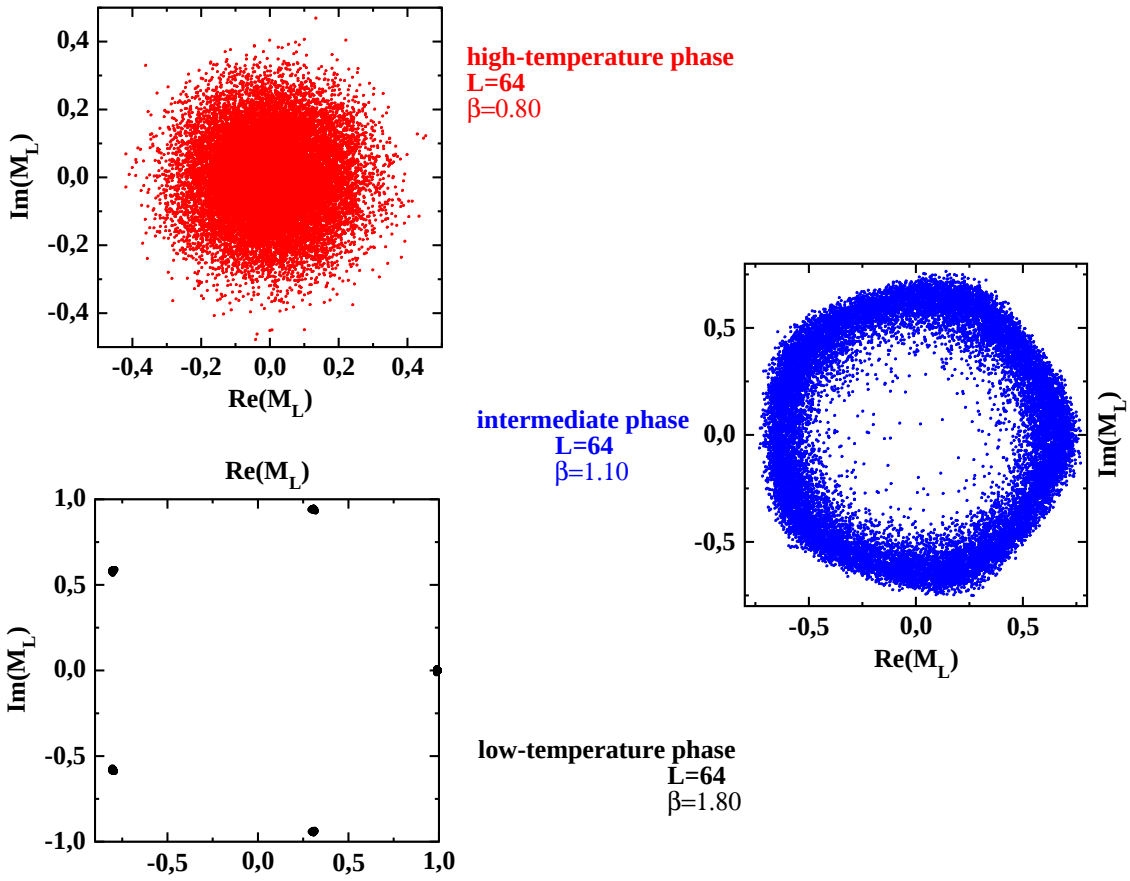

Figure 3.1: - Scatter plot of the complex magnetization M_L at $\beta = 0.80, 1.10, 1.50$ in $Z(5)$ on a 64^2 lattice.

The naive average of the complex magnetization gives constantly zero, therefore M_L is not an order parameter. An observable to detect the transition from one phase to the other is instead the absolute value $|M_L|$ of the complex magnetization and its susceptibility,

$$\chi_L^{(M)} = L^2(\langle |M_L|^2 \rangle - \langle |M_L| \rangle^2) \, , \tag{3.2}$$

As order parameter to better detect the second transition, *i.e.* that from the massless to the ordered phase, we chose instead the *population* S_L, defined as

$$S_L = \frac{N}{N-1} \left[\frac{\max_{i=0,N-1}(n_i)}{L^2} - \frac{1}{N} \right] \, , \tag{3.3}$$

where n_i represents the number of spins of a given configuration which are in the state s_i. In a phase in which there is not a preferred spin direction in the system (disorder), we have $n_i \sim L^2/N$ for each index i, therefore $S_L \sim 0$. Otherwise, in a phase in which there is a preferred spin direction (order), we have $n_i \sim L^2$ for a given index i, therefore $S_L \sim 1$ and its susceptibility

$$\chi_L^{(S)} = L^2(\langle S_L^2 \rangle - \langle S_L \rangle^2) \, , \tag{3.4}$$

Other observables which have been used in this work are the following:

- the real part of the "rotated" magnetization, $M_R = |M_L| \cos(N\psi)$,
- the order parameter introduced in Ref. (20), $m_\psi = \cos(N\psi)$,

where ψ is the phase of the complex magnetization defined in Eq. (3.1).

3.2 The Binder Cumulant

The Binder cumulant method is a very general method to compute critical exponents: it makes use of the finite-size behavior at the critical point. The basic objects, in Monte Carlo methods to study critical phenomena are renormalization-group invariant quantities, also called phenomenological couplings. In finite-size scaling (FSS) they allow to locate the transition point, to determine the nature of the transition and, in the case of a second order transition, to determine the critical exponent ν of the correlation length.

A possible choice for this quantity is the Binder cumulant defined (in general) as

$$B_4 = \frac{\sum_{xyzt}\langle s(x)s(y)s(z)s(t)\rangle}{\left[\sum_{xy}\langle s(x)s(y)\rangle\right]^2} \tag{3.5}$$

This quantity is RG invariant:

- it is a function of $\sum_x s(x)$; hence it is a long-distance quantity;
- it does not depend on the normalization of the spins; indeed, there are 4 s's in the numerator and 4 s's in the denominator;
- it is invariant under scale transformations: there is the same number of integrations over space in the numerator and in the denominator.

While the Binder cumulant is a standard tool in the study of second order transitions, only a few authors have advocated its use in the case of a KT-transition (ref.). This is due to the fact that little is known about the behavior of the Binder cumulant in the neighborhood of the KT-transition.

The fourth-order cumulant B_4, in the standard formulation can also be expressed as

$$U_L = 1 - \frac{\langle s^4\rangle_L}{3\langle s^2\rangle_L^2}. \tag{3.6}$$

This quantity becomes 2/3 in the low-temperature ordered limit, and tends towards zero in the disordered high-temperature limit. The behavior of the cumulant makes it very useful for obtaining estimates of β_c itself which are not biased by any assumptions about critical exponents. As shown in the Results chapter, finite-size scaling implies the existence of such a common intersection point. Due to corrections to finite-size scaling, there may be some scatter in the intersection point for different pairs (L, L') if one works with very small linear dimension. Nevertheless, the accuracy of this "cumulant intersection method" is quite good. So, when measured at the critical temperature, the value of the cumulant is expected to be approximately independent of the system size.

The finite-size scaling theory for first-order transitions also leads to a criterion for systematically distinguishing first-order transitions from second-order

transitions. For instance, when one computes a quantity V_L defined as (23)

$$V_L = 1 - \frac{\langle E^4 \rangle_L}{3\langle E^2 \rangle_L^2}, \tag{3.7}$$

one finds that V_L takes a minimum value V_L^{min} at the effective transition temperature $\beta_c(L)$. One can show that for a second-order transition $lim_{L\to\infty}\left[\frac{2}{3} - V_L^{min}\right] = 0$, even at β_c,while at a first-order transition the same limit measures the latent heat.

3.3 The helicity modulus

To investigate the phase transition between the BKT-like phase and the disordered phase we consider a helicity modulus Υ defined by

$$\langle \Upsilon \rangle = \frac{\partial^2 F}{\partial \Delta^2}\Big|_{\Delta=0} \tag{3.8}$$

where Δ represent an externally imposed global twist across the sample, F is the free energy $F(\Delta) = -TlnZ$ and $\langle ... \rangle$ denotes the thermal average. The helicity modulus was first introduced to study the phase transitions of isotropic spin systems, e.g. the Heisenberg model. The ordered phase of such systems has a continuos rotational symmetry in the ordered spin direction. The helicity modulus can describe the rigidity of the ordered phase against the twist. Though the ordered state in our $Z(N)$ clock models has a discrete symmetry in the lowest temperature, we expect that this model behaves similar to the XY model in the BKT-like phase and the disordered phase.

According to renormalization-group theory (3), the helicity modulus is an infinite system jumps from the finite value $(2/\pi\beta)$ to zero at the critical temperature. Assuming this applies also to the $2D$ $Z(N)$ vector models, (as argued in Ref), the critical coupling β_c from disordered to intermediate phase can be estimated from the intersection of Υ and the straight line,

$$\Upsilon = \frac{2}{\pi\beta} \tag{3.9}$$

Though the helicity modulus is defined in spin systems above, it may be applied to a Bose superfluid. In this case the helicity modulus is given by

$$\Upsilon = \left(\frac{\hbar}{m}\right)\rho_s \tag{3.10}$$

where ρ_s is a superfluid density (29).

Now, the equation $\eta = m^2 T/2\pi\hbar^2\rho_s$ between the critical exponent η of the correlation function and the superfluid density leads us to the relation (34, 35, 36)

$$\eta = \frac{1}{2\pi\beta\Upsilon}. \tag{3.11}$$

Hence we can obtain the critical exponent η through Υ without use of the finite-size scaling fitting.

4

Algorithm and Numerical Setup

In this work we concentrate our attention to the model defined by Eqs. (2.3) and (2.4), with only one non-zero coupling, $\beta_1 \equiv \beta$. This model is known in the literature also as N-state ferromagnetic clock model and is a discrete version of the continuous XY (plane rotator) model. It consists of 2D planar spins restricted to N evenly spaced directions, with spin interaction energy proportional to their scalar product.

The Hamiltonian of the model is

$$H = -\beta \sum_{\langle ij \rangle} \cos\left(\frac{2\pi}{N}(s_i - s_j)\right) \ , \qquad s_i = 0, 1, \ldots, N-1 \ , \tag{4.1}$$

with summation taken over nearest-neighbor sites. For $N = 2$ this is the Ising model, whereas in the $N \to \infty$ limit we get the XY model.

Here we develop a new algorithm, valid for odd N, by which an accurate numerical study of the model can be performed for $N = 5$, *i.e.* the smallest N value for which the phase structure described in the Introduction holds.

Here are the steps of our cluster algorithm for the update of a spin configuration $\{s_i\}$:

- choose randomly n in the set $\{0, 1, 2, \ldots, N-1\}$
- build a cluster configuration according to the following probability of bond activation between neighboring sites ij

$$p_{ij} = \begin{cases} 1 - \exp(-2\beta\ \alpha_i\alpha_j) & \text{if } \alpha_i\alpha_j > 0 \\ 0 & \text{otherwise} \end{cases} \ , \quad \text{with } \ \alpha_k \equiv \sin\left(\frac{2\pi}{N}(s_k - n)\right)$$

- "flip" each cluster, with probability 1/2, by replacing all its spins according to the transformation

$$s_i \to \mathrm{mod}(-s_i + 2n + N, N) \ ,$$

  which amounts to replacing each spin s_i in a cluster by the spin s_j for which $\alpha_j = -\alpha_i$; equivalently, if the spins are mapped into the N roots of unity in the complex plane, the above replacement means flipping the component of each spin transverse to the direction identified by n.

It is easy to prove that this cluster algorithm fulfills the detailed balance.

We have tested the efficiency of the cluster algorithm against the standard heat-bath algorithm. On a lattice with $L = 64$ we simulated the model with $N = 5$ and determined the autocorrelation time τ of three observables: the energy, defined in Eq. (4.1), the magnetization M_L and the population S_L, to be defined below. We considered three β values (0.80, 1.10 and 1.50) lying, respectively, in the high-temperature, massless and low-temperature phase of the model. Results are summarized in Table 4.1, whose last two columns give also the number of sweeps needed to reach thermal equilibrium and the computer time to collect a 50k statistics.

Table 4.1: Cluster versus heat-bath in $Z(5)$ on a 64^2 lattice at three values of β: autocorrelation time τ for three observables (energy, magnetization M_L and population S_L), number of thermalization sweeps and computer time for 50k updates.

		Energy	M_L	S_L	Thermalization	Time
$\beta = 0.80$	cluster	5.135(82)	1.528(38)	1.494(39)	~ 10	46.69 s
	heat bath	5.43(33)	12.83(27)	12.65(28)	~ 100	1290 s
$\beta = 1.10$	cluster	7.36(11)	5.56(10)	7.18(11)	~ 10	45.14 s
	heat bath	10.11(48)	48.3(4.8)	60.6(6.1)	~ 1000	1194 s
$\beta = 1.50$	cluster	8.97(17)	8.71(17)	8.84(17)	~ 100	42.60 s
	heat bath	2.38(12)	3.73(15)	3.78(13)	~ 6500	1064 s

At β=0.80 and 1.10 the autocorrelation time in the cluster algorithm is lower than in the heat-bath for the energy and much lower for magnetization and pop-

ulation. At $\beta = 1.50$, deep in the low-temperature ordered phase, τ is systematically higher in the cluster than in the heat-bath. This is a consequence of the lowering of the bond activation probability for increasing β. This drawback, however, is compensated by the higher simulation speed, with respect to the heat-bath algorithm. Moreover since the two transitions in the $2D$ $Z(5)$ model are rather close (see below), there is no doubt that the cluster algorithm is strongly preferable.

The improvement brought along by the cluster algorithm becomes more visible when the dynamical critical exponent z is considered, defined as $\tau \sim \xi^z$, where ξ is the correlation length. We have evaluated z in the $2D$ $Z(5)$ model on lattices with $L = 16, 32, 64, 128, 256, 384, 512$ at both transition points, using the autocorrelation time of the magnetization M_L. Since at both points the correlation length diverges, the expected scaling law becomes $\tau \sim L^z$. We got in all cases that τ keeps almost constant at ≈ 7, thus implying $z \simeq 0$, *i.e.* no critical slowing down.

For all observables considered in this work we collected typically 100k measurements, on configurations separated by 10 updating sweeps. For each new run the first 10k configurations were skipped for the purpose of bringing the system to thermal equilibrium for both the small and large lattices. Data analysis was performed by the jackknife method over bins at different blocking levels.

5

Results

5.1 The $2D$ $Z(5)$ vector model: from disordered to massless phase

In Figs. 5.1 and 5.2 we show the behavior of $|M_L|$ and of its susceptibility, in $Z(5)$ on lattices with L ranging from 16 to 1024 over a wide interval of β values. On each lattice the susceptibility $\chi_L^{(M)}$ clearly exhibits two peaks, the first of them, more pronounced than the other, identifies the pseudocritical coupling $\beta_{\rm pc}^{(1)}(L)$ at which the transition from the disordered to the massless phase occurs, whereas the second corresponds to the pseudocritical coupling $\beta_{\rm pc}^{(2)}(L)$ of the transition from the massless to the ordered phase. It is evident from Fig. 5.1 that $|M_L|$ is particularly sensitive to the first transition, thus making this observable the best candidate for studying its properties.

The first inflection point in the plot of the magnetization $|M_L|$ and the first peak in the plot of the susceptibility $\chi_L^{(M)}$ (see Figs. 5.1, 5.2) indicate the transition from the disordered to the massless phase. The couplings where this transition occurs (denoted as the pseudocritical couplings $\beta_{\rm pc}^{(1)}(L)$) have been determined by a Lorentzian interpolation around the peak of the susceptibility $\chi_L^{(M)}$. Their values are summarized in the second column of Table 5.1. We observe that, when the lattice size L grows, $\beta_{\rm pc}^{(1)}(L)$ increases towards the infinite volume critical coupling $\beta_{\rm c}^{(1)}$ and that the susceptibility $\chi_L^{(M)}$ goes to zero less rapidly for $\beta > \beta_{\rm pc}^{(1)}$, as expected in the BKT scenario.

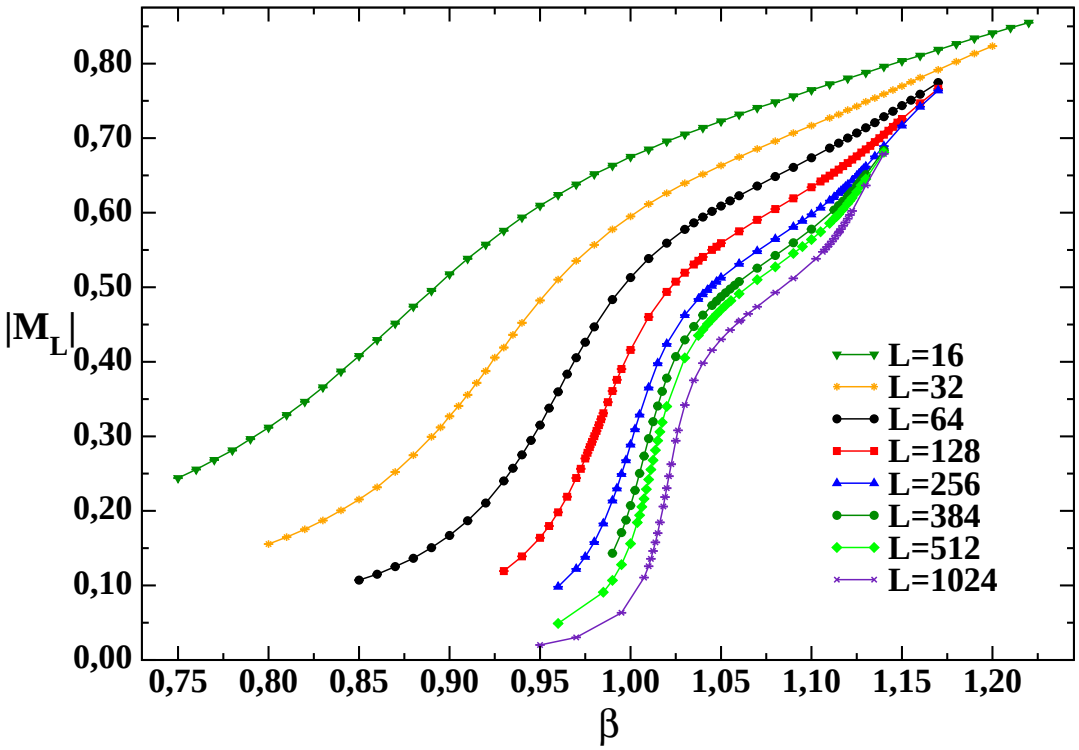

Figure 5.1: - Behavior of $|M_L|$ versus β in $Z(5)$ on lattices with L ranging from 16 to 1024.

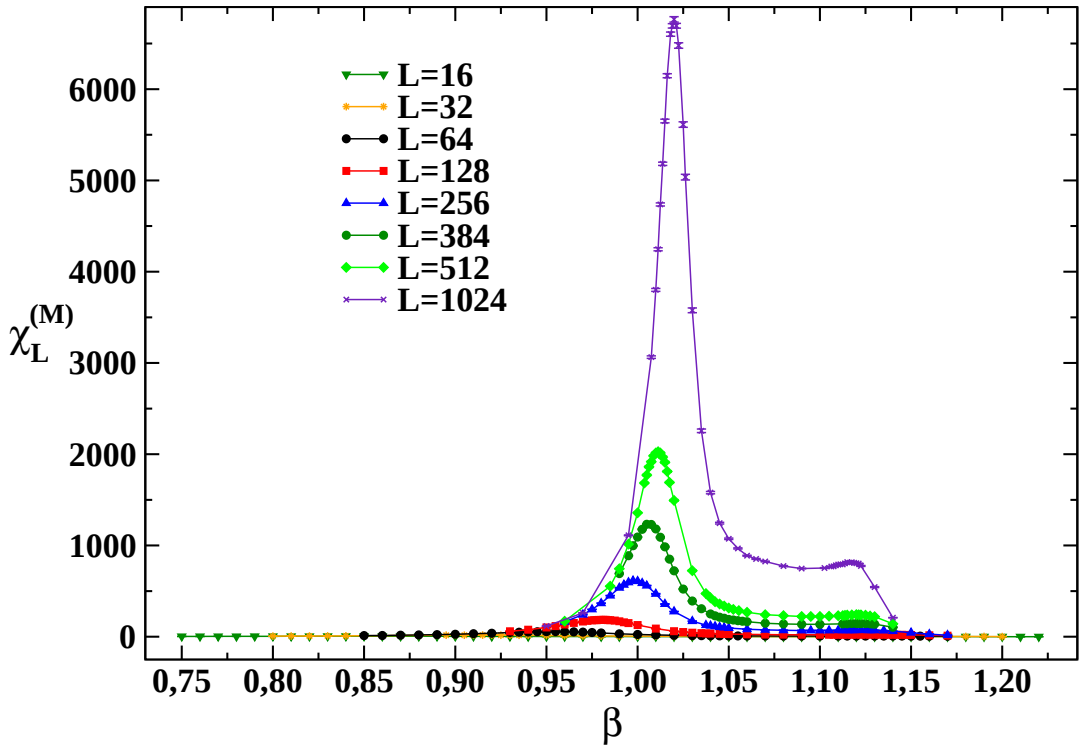

Figure 5.2: - Susceptibility $\chi_L^{(M)}$ versus β in $Z(5)$ on lattices with L ranging from 16 to 1024.

Table 5.1: Values of $\beta_{\rm pc}^{(1)}$ in $Z(5)$ on L^2 lattices. The last two columns give the susceptibility $\chi_L^{(M)}$ and the magnetization $|M_L|$ at the infinite volume coupling constant $\beta_{\rm c}^{(1)}$=1.0510.

L	$\beta_{\rm pc}^{(1)}$	$\chi_L^{(M)}(\beta_{\rm c}^{(1)})$	$\lvert M_L\rvert(\beta_{\rm c}^{(1)})$
16	0.8523(20)	-	-
32	0.91429(90)	-	-
64	0.95373(40)	-	-
128	0.98054(30)	-	-
256	0.99838(20)	-	-
384	1.00621(10)	187.9(1.2)	0.48929(13)
512	1.01112(20)	311.5(2.0)	0.47181(13)
640	-	458.6(3.4)	0.45918(11)
768	-	631.3(4.2)	0.44863(11)
896	-	824.4(5.2)	0.44004(11)
1024	1.01991(10)	1040.0(6.9)	0.43277(11)

In order to apply the finite size scaling (FSS) program, the location of the infinite volume critical coupling $\beta_c^{(1)}$ is needed. In Refs. (24, 25) this was done by extrapolating the pseudocritical couplings to the infinite volume limit, according to a suitable scaling law. First order transition is ruled out by data in Table 5.1. Second order transition, though not incompatible with data in Table 5.1, is to be excluded, due to the vanishing of the long distance correlations combined with the clusterization property (we will come back to this point in the last Section). Therefore, we assume that the transition is of BKT type and adopt the scaling law dictated by the essential scaling of the BKT transition, *i.e.* $\xi \sim e^{bt^{-\nu}}$, which reads

$$\beta_{\rm pc}^{(1)} = \beta_{\rm c}^{(1)} + \frac{A}{(\ln L + B)^{\frac{1}{\nu}}} \quad . \tag{5.1}$$

The index ν characterizes the universality class of the system. For example, $\nu = 1/2$ holds for the $2D$ XY universality class.

Unfortunately, 4-parameter fits of the data for $\beta_{\rm pc}^{(1)}(L)$ give very unstable results for the parameters. This led us to move to 3-parameter fits of the data,

with ν fixed at 1/2. We found, as best fit with the MINUIT optimization code,

$$\beta_{\rm c}^{(1)} = 1.0602(20)\ ,\quad A_1 = -2.09(20)\ ,\quad B_1 = 0.27(18)\ ,\quad \chi^2/\text{d.o.f.} = 0.48\ ,\quad L_{\rm min} = 64\ .$$

We observe that $\beta_{\rm c}^{(1)}$ is rather far from the value of $\beta_{\rm pc}^{(1)}$ on the largest available lattice, thus casting some doubts on the reliability of the extrapolation to the thermodynamic limit. For this reason, we turned to an independent method for the determination of $\beta_{\rm c}^{(1)}$, based on the use of Binder cumulants.

In particular, we considered the *reduced* 4-th order Binder cumulant $U_L^{(M)}$ defined as

$$U_L^{(M)} = 1 - \frac{\langle |M_L|^4 \rangle}{3\langle |M_L|^2 \rangle^2}\ , \tag{5.2}$$

and the cumulant $B_4^{(M_R)}$ defined as

$$B_4^{(M_R)} = \frac{\langle |M_R - \langle M_R \rangle|^4 \rangle}{\langle |M_R - \langle M_R \rangle|^2 \rangle^2}\ . \tag{5.3}$$

Plots of the various Binder cumulants versus β show that data obtained on different lattice volumes align on curves that cross in two points, corresponding to the two transitions (see Figs. 5.3 and 5.4). We used also the *reduced* 4-th order Binder cumulant of the action which showed no crossing points nor volume-dependent dips, thus confirming the absence of first order phase transitions.

We determined the crossing point by plotting the Binder cumulants versus $(\beta - \beta_{\rm c})(\log L)^{1/\nu}$, with ν fixed at 1/2, and by looking for the optimal overlap of data from different lattices, by the χ^2 method (see Fig. **??** for an example of this kind of plots). As a result of this analysis we arrived at the following estimate: $\beta_{\rm c}^{(1)} = 1.0510(10)$. We observe that $\beta_{\rm c}^{(1)}$ is not compatible with the infinite volume extrapolation of the corresponding pseudocritical couplings, thus confirming our previous worries about the safety of the infinite volume extrapolation of $\beta_{\rm pc}^{(1)}$. It should be noted, however, that a fit to $\beta_{\rm pc}^{(1)}(L)$ with the law (5.1) and with $\beta_{\rm c}^{(1)}$ fixed at 1.0510 and ν fixed at 1/2 gives a good χ^2/d.o.f., if only the three largest volumes are considered in the fit.

We are now in the position to extract other critical indices and check therefore the hyperscaling relation. According to the standard FSS theory, in a $L \times L$ lattice at criticality the equilibrium magnetization $|M_L|$ should obey the relation

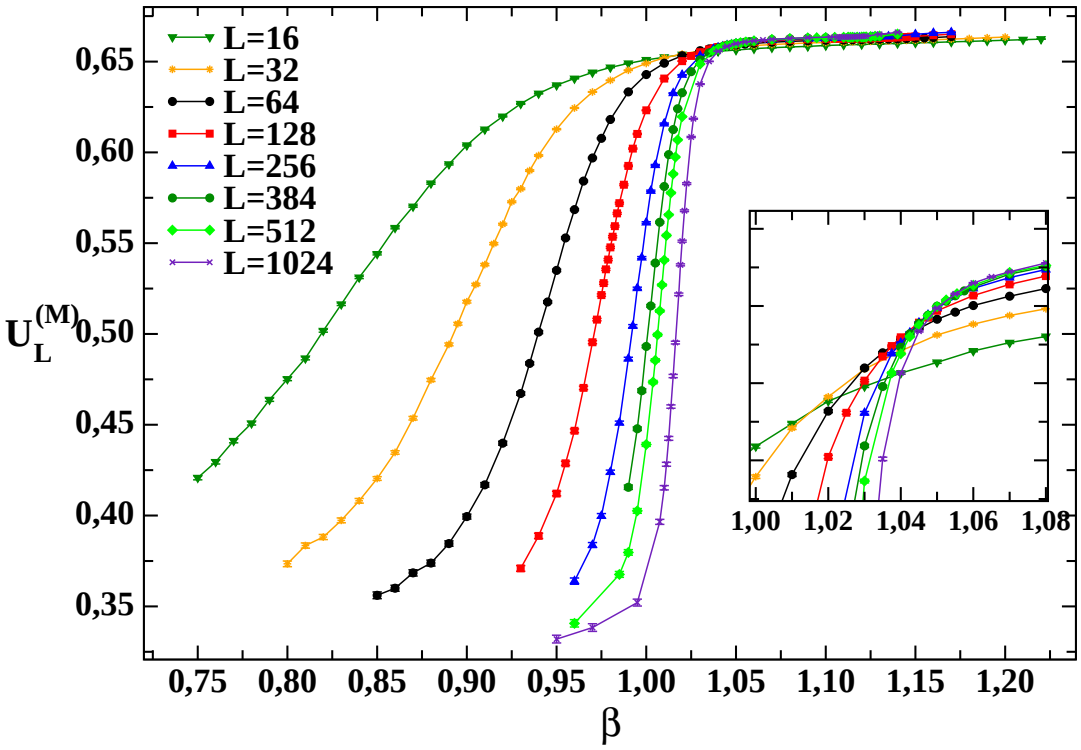

Figure 5.3: - Reduced 4-th order Binder cumulant $U_L^{(M)}$ versus β on lattices with L ranging from 16 to 1024.

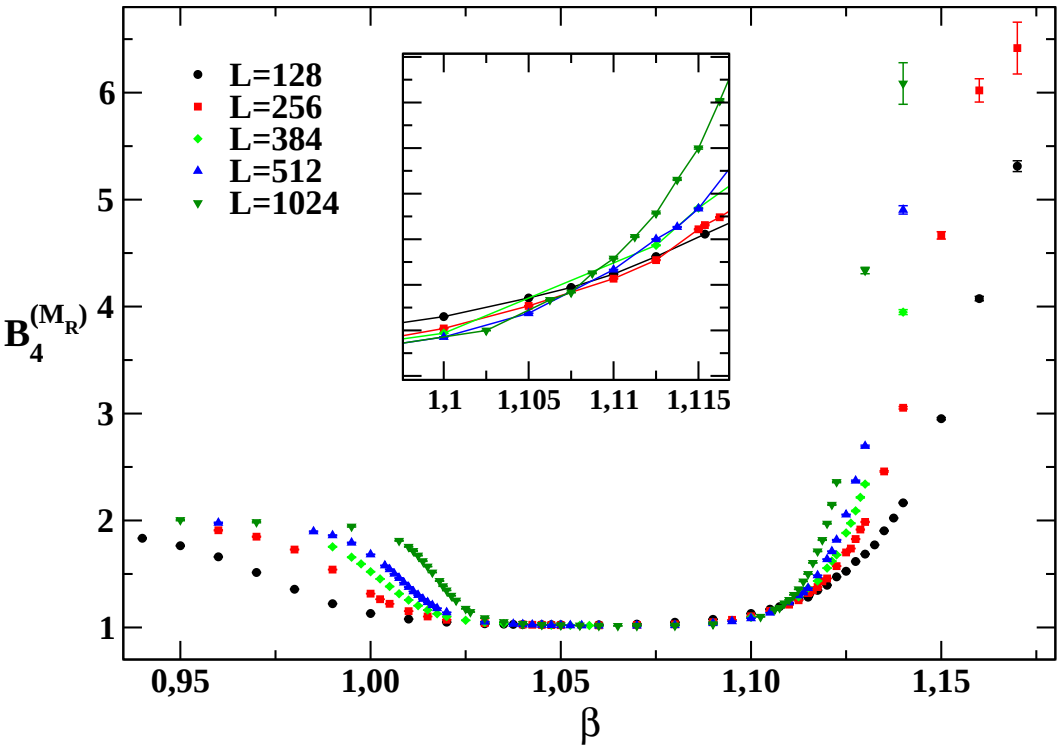

Figure 5.4: - Binder cumulant $B_4^{(M_R)}$ versus β on lattices with L ranging from 128 to 1024.

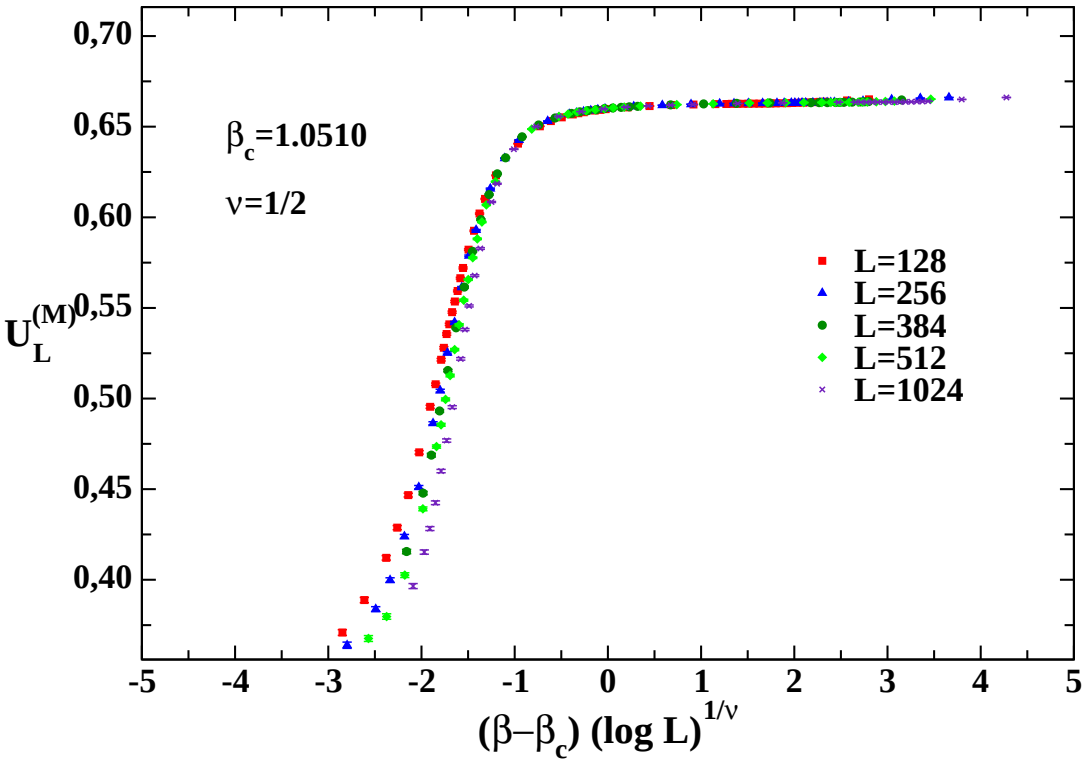

Figure 5.5: - Reduced 4-th order Binder cumulant $U_L^{(M)}$ versus $(\beta-\beta_c)(\log L)^{1/\nu}$, for $\beta_c = 1.0510$ and $\nu = 1/2$ on lattices with L ranging from 128 to 1024.

Table 5.2: Results of the fit to the data of $|M_L|(\beta_c^{(1)})$ with the scaling law (5.4) on L^2 lattices with $L \geq L_{\min}$.

$L_{\min}$	A	β/ν	χ^2/d.o.f.
384	1.0299(21)	0.12508(32)	1.3
512	1.0294(32)	0.12501(47)	1.7
640	1.0371(49)	0.12610(71)	0.40
768	1.0305(89)	0.1252(13)	0.021

Table 5.3: Results of the fit to the data of $\chi_L^{(M)}(\beta_c^{(1)})$ with the scaling law (5.5) on L^2 lattices with $L \geq L_{\min}$.

$L_{\min}$	A	γ/ν	χ^2/d.o.f.
384	0.00586(30)	1.7438(80)	0.060
512	0.00602(48)	1.740(12)	0.018
640	0.00598(81)	1.741(20)	0.025
768	0.0062(14)	1.735(34)	0.0063

$|M_L| \sim L^{-\beta/\nu}$, for sufficiently large L [1]. We performed a fit to the data of $|M_L|(\beta_c^{(1)})$ (reported in the last column of Table 5.1) on all lattices with size L not smaller than a given $L_{\min}$ according to the scaling law

$$|M_L| = AL^{-\beta/\nu} \tag{5.4}$$

and summarized our results in Table 5.2.

The FSS behavior of the $\chi_L^{(M)}$ susceptibility defined in Eq. (3.2) is given by $\chi_L^{(M)} \sim L^{\gamma/\nu}$, where $\gamma/\nu = 2 - \eta$ and η is the magnetic critical index. We performed a fit to the data of $\chi_L^{(M)}(\beta_c^{(1)})$ (reported in the third column of Table 5.1) on all lattices with size L not smaller than a given $L_{\min}$ according to the scaling law

$$\chi_L^{(M)} = AL^{\gamma/\nu} \tag{5.5}$$

[1] The symbol β here denotes a critical index and not, obviously, the coupling of the theory. In spite of this inconvenient notation, we are confident that no confusion will arise, since it will be always clear from the context which β is to be referred to.

and summarized our results in Table 5.3. As we can see, for all values of $L_{\min}$ considered, the value of the magnetic index [1] $\eta^{(1)} \equiv 2 - \gamma/\nu$ is compatible with 1/4. Note also that the hyperscaling relation $\gamma/\nu + 2\beta/\nu = d$, where d is the dimension of the system, is always satisfied within the statistical error.

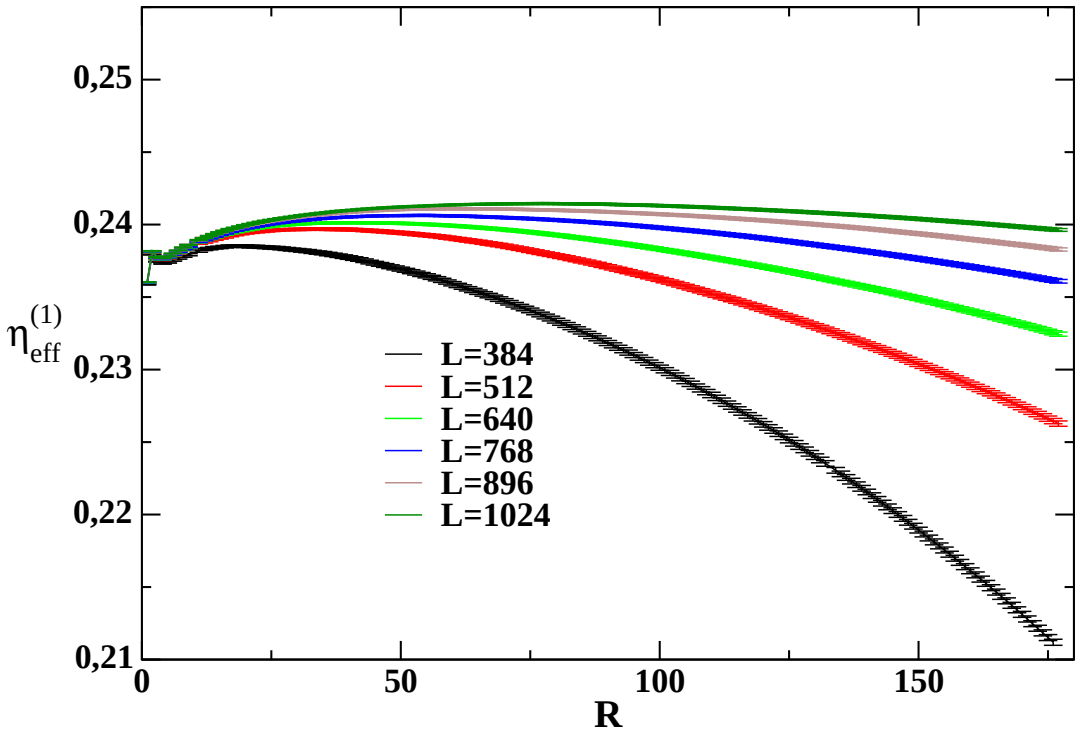

Figure 5.6: - $\eta^{(1)}_{\rm eff}$ versus R at $\beta_c^{(1)} = 1.0510$ on lattices with $L = 384, 512, 640, 768, 896, 1024$.

An independent determination of the magnetic index η can be achieved by the approach developed in Ref. (24): an *effective* η index is defined, through the spin-spin correlation function $\Gamma(R)$, according to

$$\eta^{(1)}_{\rm eff}(R) \equiv \frac{\log[\Gamma(R)/\Gamma(R_0)]}{\log[R_0/R]} \quad , \tag{5.6}$$

[1] The notation $^{(1)}$ in η means "at the infinite volume critical coupling of the *first* transition".

with R_0 chosen equal to 10, as in Ref. (24). This quantity is constructed in such a way that it exhibits a *plateau* in R if the correlator obeys the law

$$\Gamma(R) \asymp \frac{1}{R^{\eta(T)}} , \tag{5.7}$$

valid in the BKT phase, $\beta \geq \beta_c^{(1)}$. In Fig. **??** we show the behavior of $\eta_{\rm eff}^{(1)}(R)$ at the infinite volume critical coupling $\beta_c^{(1)} = 1.0510$ on lattices with $L = 384, 512, 640, 768, 896, 1024$. It turns out that a plateau develops at small distances when L increases and that the extension of this plateau gets larger with L, consistently with the fact that finite volume effects are becoming less important. The plateau value of $\eta_{\rm eff}^{(1)}$ can be estimated at about 0.24. We checked that this result is stable under variation of the parameter R_0. The discrepancy with the expected value of 1/4 can be explained by the imperfect localization of the critical point and/or by the effect of logarithmic corrections (26, 27) that we were not able to include in our analysis.

Table 5.4: Values of $\beta_{\rm pc}^{(2)}$ in $Z(5)$ on L^2 lattices. The last two columns give the susceptibility $\chi_L^{(M_R)}$ and the rotated magnetization M_R at the infinite volume coupling constant $\beta_c^{(2)}$=1.1048.

L	$\beta_{\rm pc}^{(2)}$	$\chi_L^{(M_R)}(\beta_c^{(2)})$	$M_R(\beta_c^{(2)})$
16	1.1323(19)	-	-
32	1.1363(11)	-	-
64	1.13212(60)	-	-
128	1.12875(66)	-	-
256	1.12290(16)	-	-
384	1.12103(50)	47116(77)	0.1618(18)
512	1.11912(28)	80057(139)	0.1575(19)
640	-	120777(229)	0.1557(20)
768	-	169358(298)	0.1517(19)
896	-	224879(339)	0.1502(16)
1024	1.11596(38)	288151(532)	0.1473(18)

5.2 The $2D$ $Z(5)$ vector model: from massless to ordered phase

In Figs. 5.7 and 5.8 we show the behavior of S_L and of its susceptibility in $Z(5)$ on lattices with L ranging from 16 to 1024 over a wide interval of β values. Again the peaks signalling the two transitions are clearly visible and their positions agree with Figs. 5.1, 5.2, but now the second one is more pronounced.

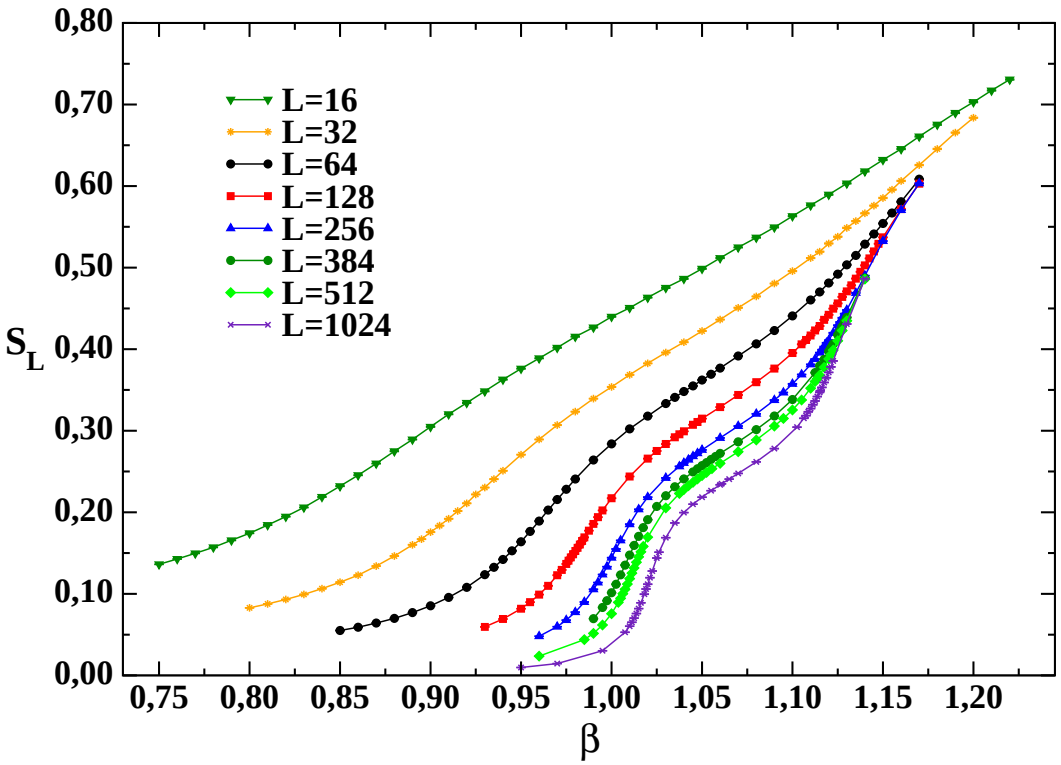

Figure 5.7: - Population

The second inflection point in the plot of the population S_L and the second peak in the plot of the susceptibility $\chi_L^{(S)}$ (see Fig. 5.7, 5.8) indicate the transition from the massless to the ordered phase. The couplings where this transition

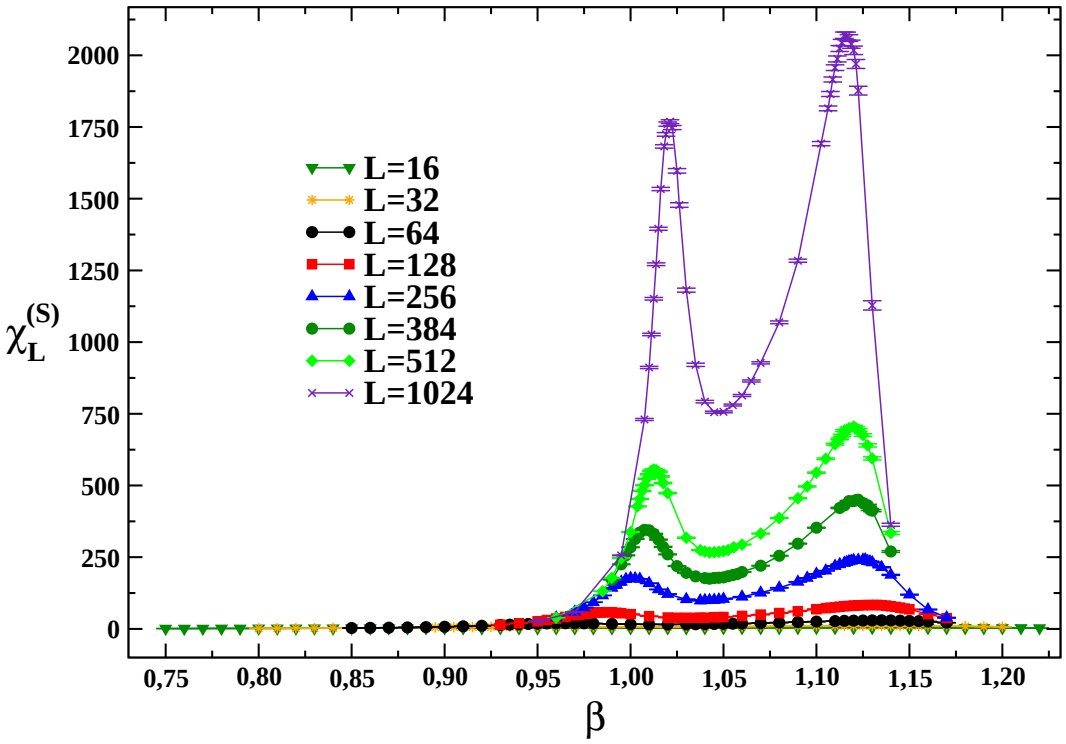

Figure 5.8: - Suscet

occurs (denoted as the pseudocritical couplings $\beta_{\rm pc}^{(2)}(L)$) have been determined by a Lorentzian interpolation around the peak of the susceptibility $\chi_L^{(S)}$. Their values are summarized in the second column of Table 5.4.

Available results in the literature (5, 11) suggest that the correlation length diverges according to essential scaling scenario when the critical point is approached from above. Our aim is to check the validity of this statement and then extract relevant indices characterizing the system at this transition. Again, first order transition is ruled out by data in Table 5.4 (and by the aforementioned analysis of the Binder cumulant of the action), while second order is not. We assume that a BKT transition is at work here and, therefore, that pseudocritical couplings scale with L according to the law (5.1). As before, 4-parameter fits of the data for $\beta_{\rm pc}^{(2)}(L)$ are unstable and we moved to 3-parameter fits of the data, with ν fixed at 1/2, finding that the parameter B_2 turns out to be compatible with zero, so that, in fact, a 2-parameter fit works well:

$$\beta_{\rm c}^{(2)} = 1.1042(12)\ ,\quad A_2 = 0.578(41)\ ,\quad B_2 = 0.\ ,\quad \chi^2/\text{d.o.f.} = 0.61\ ,\quad L_{\rm min} = 128\ .$$

Now $\beta_{\rm c}^{(2)}$ is not far from the value of $\beta_{\rm pc}^{(2)}$ on the largest available lattice, thus supporting the reliability of the extrapolation to the thermodynamic limit.

Table 5.5: Results of the fit to the data of $\chi_L^{(M_R)}(\beta_{\rm c}^{(2)})$ with the scaling law (5.5) on L^2 lattices with $L \geq L_{\rm min}$.

$L_{\rm min}$	A	γ/ν	χ^2/d.o.f.
384	0.799(11)	1.8459(21)	0.23
512	0.791(17)	1.8473(32)	0.19
640	0.784(28)	1.8487(53)	0.22
768	0.793(50)	1.8470(92)	0.39

In order to localize the critical coupling $\beta_{\rm c}^{(2)}$, we looked for the crossing point at higher β of the Binder cumulant $B_4^{(M_R)}$ defined in Eq. (5.4) and repeated the analysis based on the optimal overlap of data points when they are plotted against $(\beta - \beta_{\rm c})(\log L)^{1/\nu}$, with ν fixed at 1/2. The same procedure was carried on using also the observable m_ψ, which is itself an RG-invariant quantity and shares therefore the same properties of a Binder cumulant (see Fig. 5.9 for the

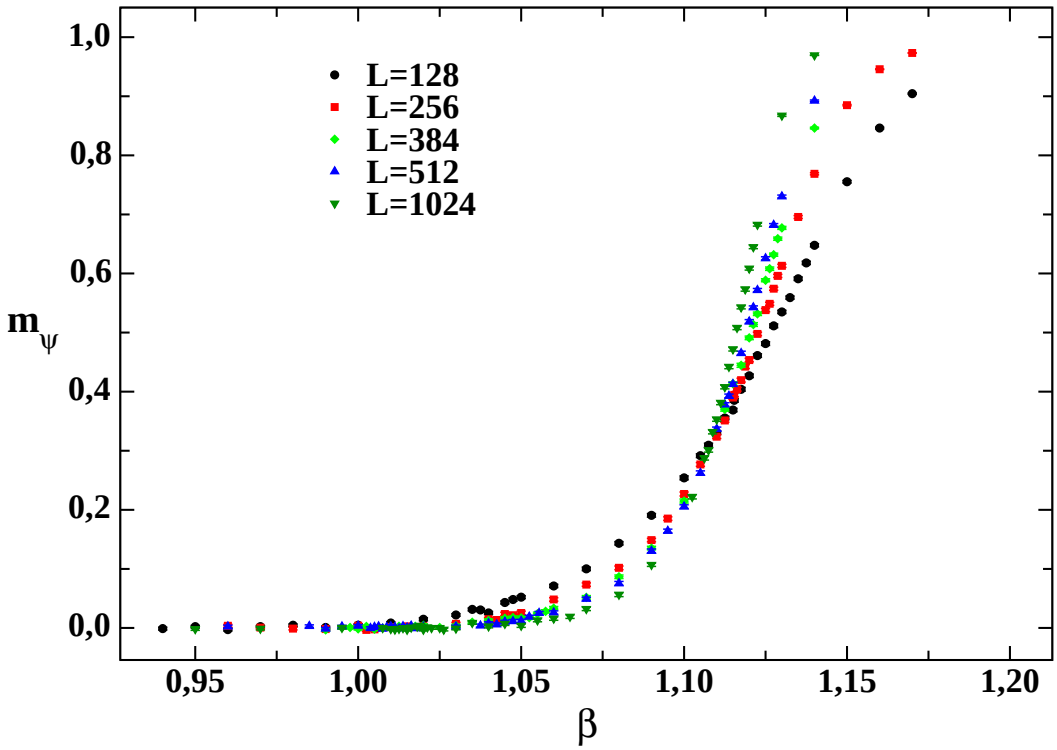

Figure 5.9: - Behavior of m_ψ versus β on lattices with L ranging from 128 to 1024.

Table 5.6: Results of the fit to the data of $M_R(\beta_c^{(2)})$ with the scaling law (5.4) on L^2 lattices with $L \geq L_{\min}$.

$L_{\min}$	A	β/ν	χ^2/d.o.f.
384	0.281(26)	0.093(14)	0.15
512	0.288(41)	0.096(22)	0.18
640	0.322(77)	0.112(36)	0.12
768	0.30(12)	0.102(60)	0.19

behavior of m_ψ versus β on various lattices, which shows two crossing points, the one at higher β corresponding to the transition from the massless to the ordered phase). This analysis led to the result $\beta_c^{(2)} = 1.1048(10)$, which agrees with the infinite volume extrapolation of the corresponding pseudocritical couplings.

We can now determine the ratios of critical indices β/ν and γ/ν as we did in the previous Section. It should be noted, however, that the population S_L and its susceptibility are not suitable observables for this purpose, being defined in a non-local manner and, thus, not directly related to the two-point correlator. We use, instead, the rotated magnetization M_R and its susceptibility $\chi_L^{(M_R)}$ and compare their values at the infinite volume critical coupling $\beta_c^{(2)}$ (see the last two columns of Table 5.4) with the scaling laws (5.4) and (5.5), respectively. Results for β/ν and γ/ν are summarized in Tables 5.5 and 5.6.

All the values for $\eta^{(2)} = 2 - \gamma/\nu$ given in Table 5.5 are in agreement with the prediction $4/N^2$, which gives 0.16 for $N = 5$. The hyperscaling relation $\gamma/\nu + 2\beta/\nu = d$ is always satisfied, within the statistical error.

The determination of the magnetic critical index based on the effective η index defined in (5.6) is plagued, in this region of values of β, by a sizeable dependence on the choice of the arbitrary parameter R_0. The shape of the curves for $\eta_{\text{eff}}(R)$ and the way they depend on R_0 suggest that here logarithmic corrections to the scaling could be at work. However, our data are not accurate enough to include them reliably in our fits.

We conclude this Section by presenting several examples of *a posteriori* check of consistency of our determinations for $\eta^{(1)}$ and $\eta^{(2)}$. The basic idea is to build plots in which we correlate two RG-invariant quantities and to check that se-

quences of data points, corresponding to different values of β, fall on a universal curve, irrespective of the lattice size L (23, 28).

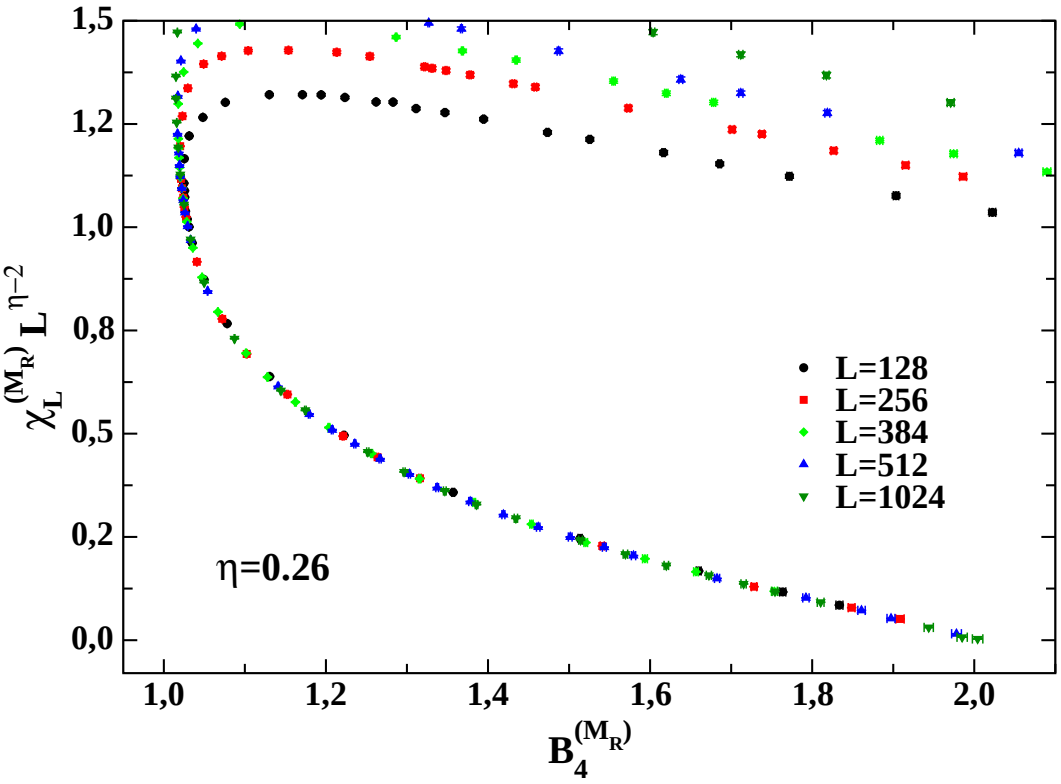

Figure 5.10: - Correlation between $\chi_L^{(M_R)} L^{\eta-2}$ and the Binder cumulant $B_4^{(M_R)}$ for $\eta = 0.26$ on lattices with L ranging from 128 to 1024. Data from different lattices tend to fall on a universal curve in the lower branch, corresponding to β values in the region of the first transition.

The first example is the plot of the rescaled susceptibility $\chi_L^{(M_R)} L^{\eta-2}$ against the Binder cumulant $B_4^{(M_R)}$. One can see from Fig. 5.10(a) that for $\eta = 0.26 \simeq \eta^{(1)}$ data points from different lattices fall on the same curve in the lower branch, corresponding to β values in the region of the first transition; for $\eta = 0.16 \simeq \eta^{(2)}$ (see Fig. 5.11), on the contrary, data points from different lattices fall on the same curve in the upper branch, corresponding to β values in the region of the

second transition (see Fig. 5.11).

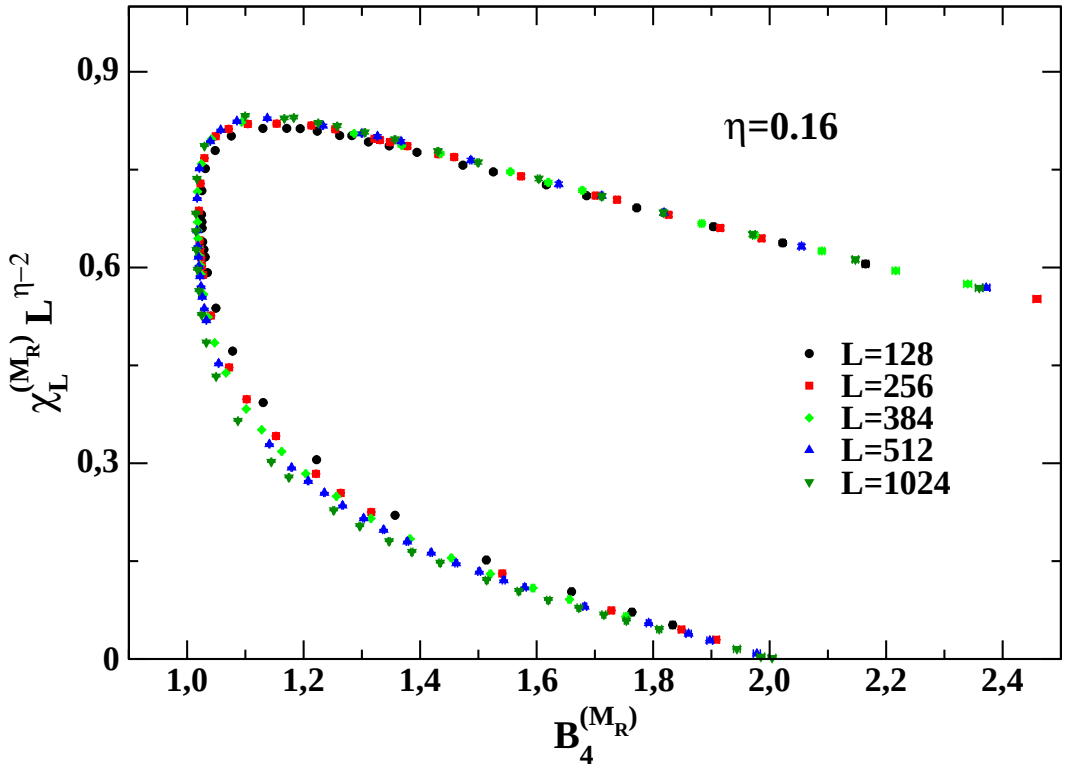

Figure 5.11: - Correlation between $\chi_L^{(M_R)} L^{\eta-2}$ and the Binder cumulant $B_4^{(M_R)}$ for $\eta = 0.16$ on lattices with L ranging from 128 to 1024. Data from different lattices tend to fall on a universal curve in the upper branch, corresponding to β values in the region of the second transition.

Another example is provided by the plot of the rescaled magnetization $M_R L^{\eta/2}$ against m_ψ. For $\eta = 0.16 \simeq \eta^{(2)}$, again data points from different lattices fall on the same curve (see Fig. 5.12).

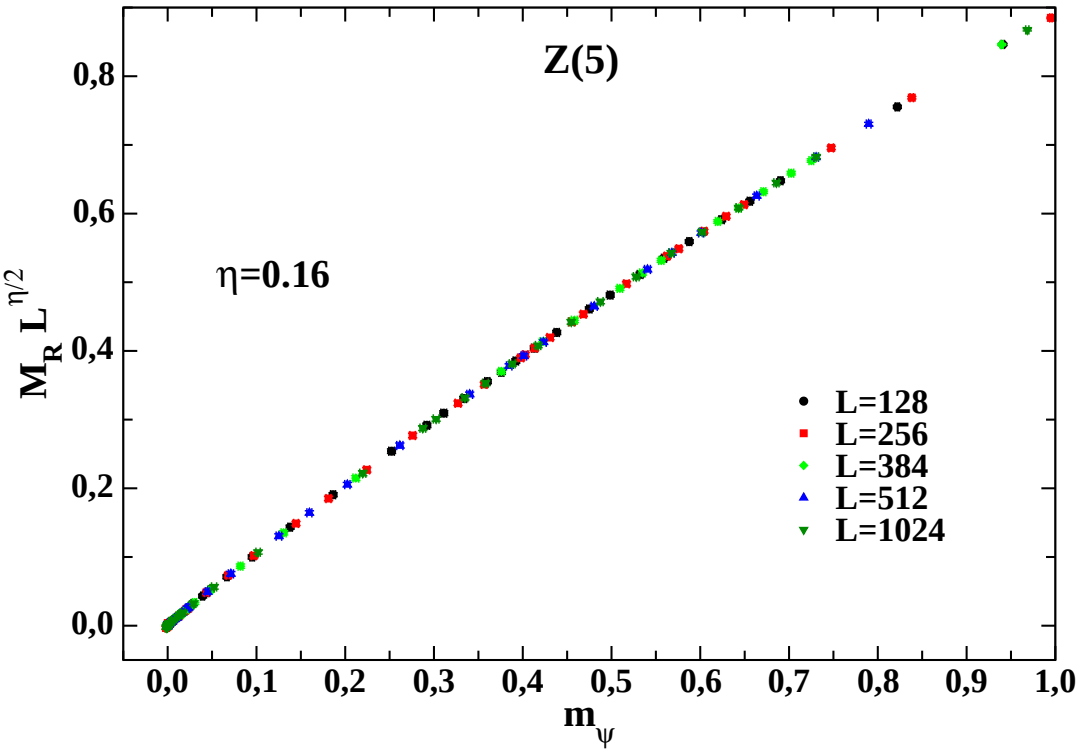

Figure 5.12: - Correlation between $M_R L^{\eta/2}$ and m_ψ for $\eta = 0.16$ on lattices with L ranging from 128 to 1024.

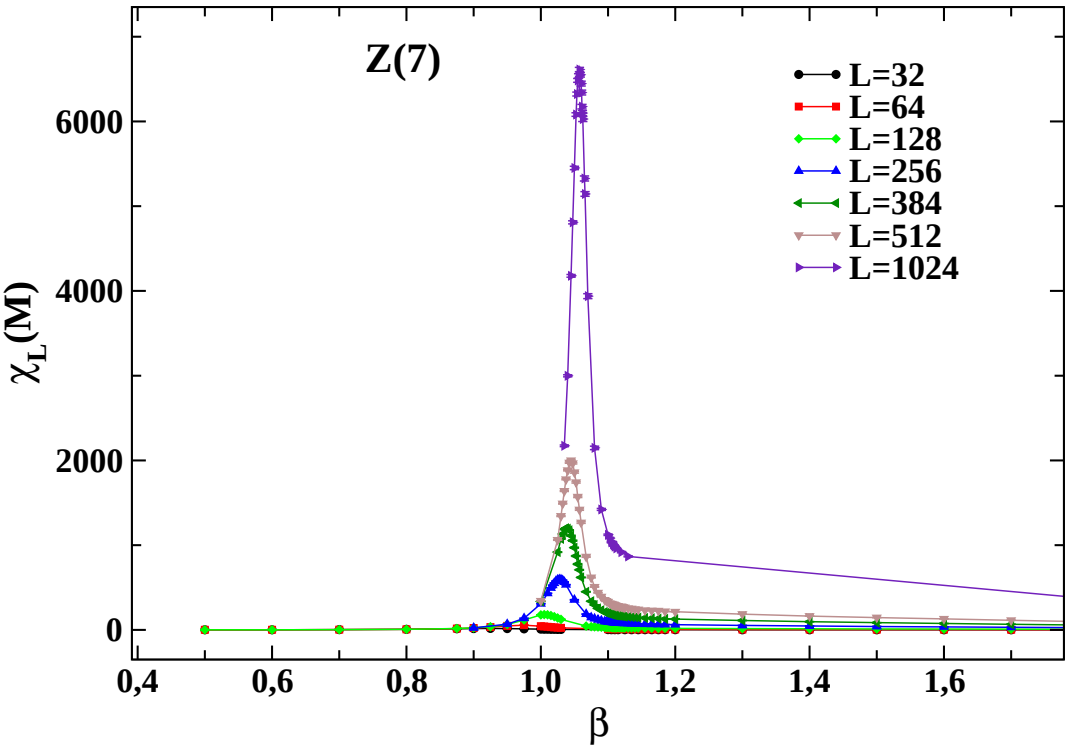

Figure 5.13: - Susceptibility $\chi_L^{(M)}$ versus β in $Z(7)$ on lattices with several values of L.

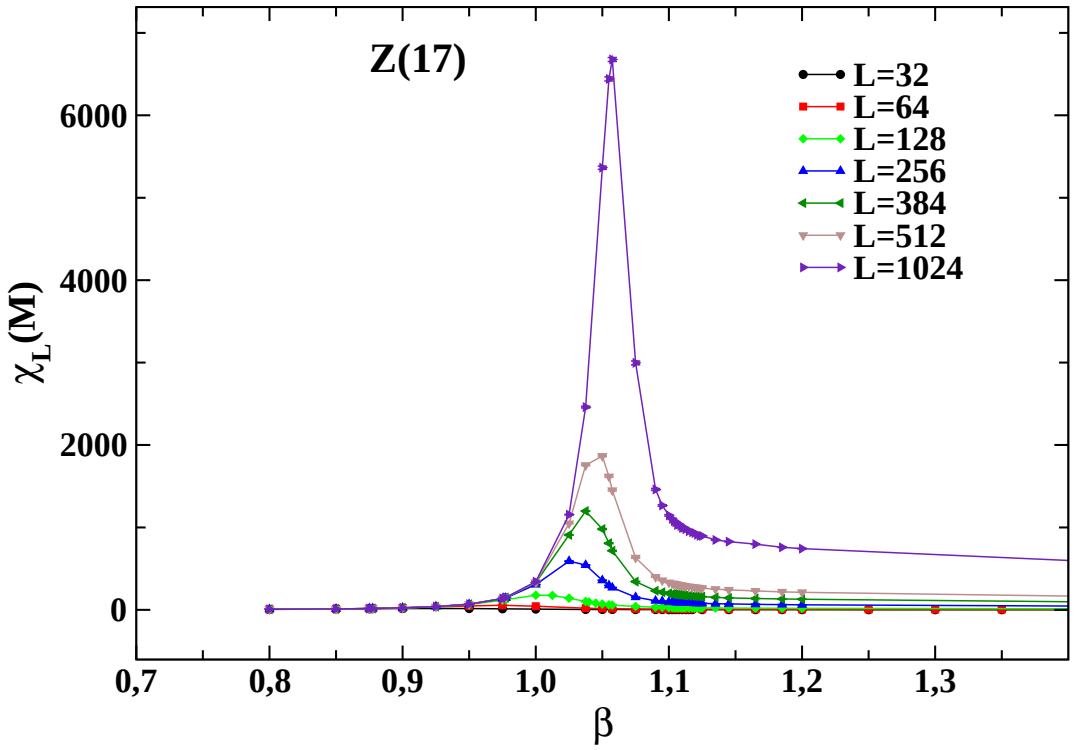

Figure 5.14: - Susceptibility $\chi_L^{(M)}$ versus β in $Z(17)$ on lattices with several values of L.

5.3 The $2D$ $Z(7)$ & $Z(17)$ vector models

After the understanding the phase diagram of the $2D$ $Z(5)$ vector model we extend the study on the $2D$ $Z(7)$ and $Z(17)$ models.

First of all I want to show you how quantities like the the susceptibilities of the absolute value of the complex magnetization $\chi_L^{(M)}$ and the parameter m_ψ behaves in these systems.

In Figs. 5.13, 5.14 we show, for both models, the behavior of the susceptibility $\chi_L^{(M)} \equiv L^2(\langle|M_L|^2\rangle - \langle|M_L|\rangle^2)$ of the absolute value of the complex magnetization, which exhibits, for each volume considered, a clear peak signalling the first phase transition. The position of the peak in the thermodynamic limit defines the first critical coupling, $\beta_c^{(1)}$. Figs. 5.15, 5.16 shows instead the behavior of m_ψ versus β on various lattice sizes; here the second critical coupling $\beta_c^{(2)}$ is identified by the crossing point (in the thermodynamic limit) of the curves formed by the data on different lattice sizes.

To determine the first critical coupling $\beta_c^{(1)}$, we could extrapolate to infinite volume the pseudo-critical couplings given by the position of the peaks of $\chi_L^{(M)}$. However, since the approach to the thermodynamic limit is rather slow (powers of $\log L$), we adopted a different method, based on the use of the "*reduced fourth-order*" Binder cumulant $U_L^{(M)}$ (see formula 5.2), the cumulant $B_4^{(M_R)}$ (formula 5.4) and the helicity modulus Υ defined in the next section. We estimated $\beta_c^{(1)}$ by looking for (i) the crossing point of the curves, obtained on different volumes, giving a Binder cumulant versus β and (ii) the optimal overlap of the same curves after plotting them versus $(\beta - \beta_c)(\log L)^{1/\nu}$, with ν fixed at $1/2$. The method (ii) has been applied also to the helicity modulus Υ.

Our best values for $\beta_c^{(1)}$ are

$$N = 7: \qquad \beta_c^{(1)} = 1.1113(13)\ ,$$
$$N = 17: \qquad \beta_c^{(1)} = 1.11375(250)\ .$$

Then, we performed the finite size scaling (FSS) analysis of the magnetization $|M_L|$ and the susceptibility $\chi_L^{(M)}$ at $\beta_c^{(1)}$ using the following laws:

$$|M_L|(\beta_c^{(1)}) = AL^{-\beta/\nu}\ , \tag{5.8}$$

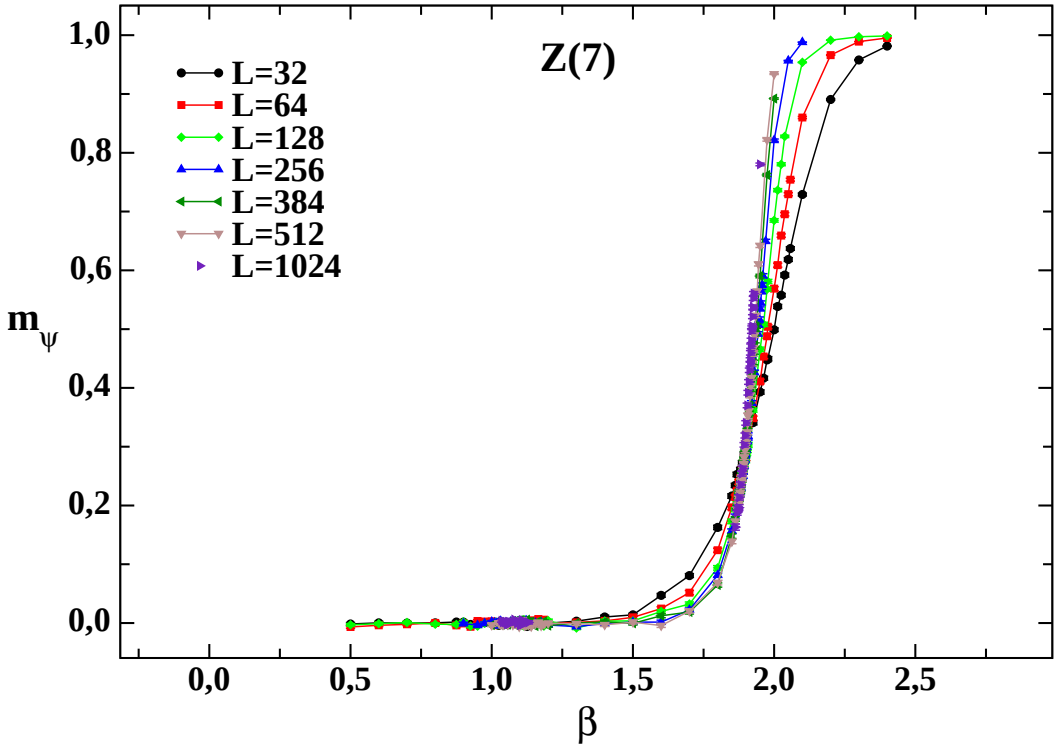

Figure 5.15: - Behavior of m_ψ with β in $Z(7)$ on lattices with several values of L.

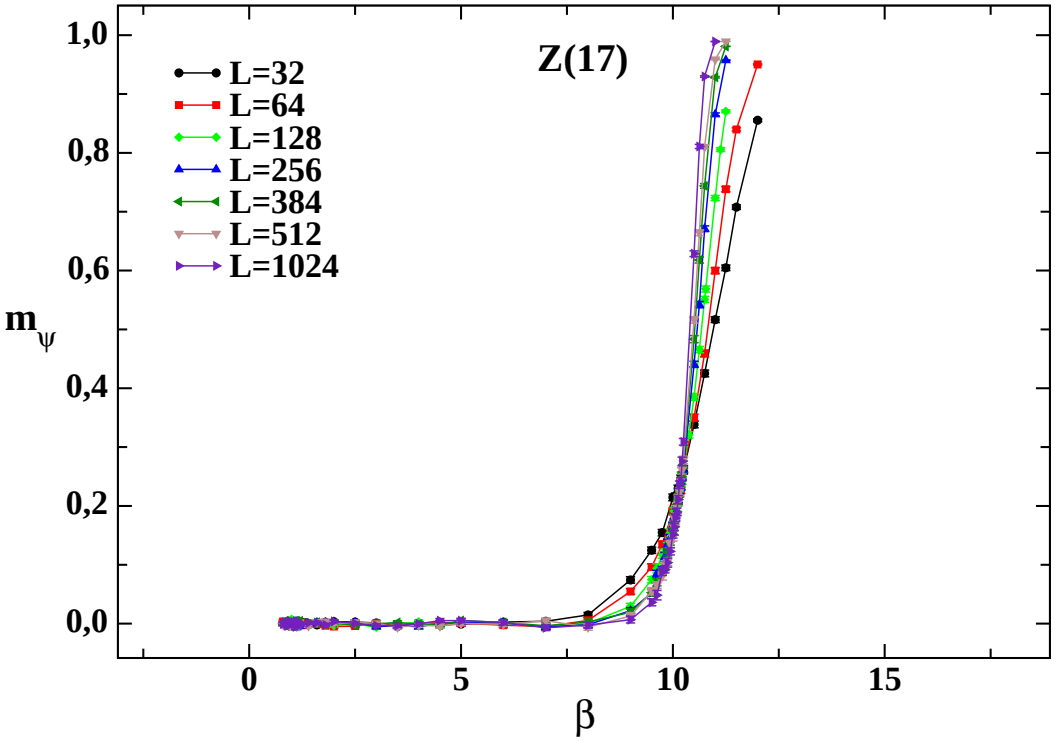

Figure 5.16: - Behavior of m_ψ with β in $Z(17)$ on lattices with several values of L.

$$\chi_L^{(M)}(\beta_c^{(1)}) = BL^{\gamma/\nu} \,, \tag{5.9}$$

where $\gamma/\nu = 2 - \eta$ and η is the *magnetic critical index*. Results are summarized in Tables 5.7, 5.8, 5.9 and 5.10. We observe that the hyperscaling relation $\gamma/\nu + 2\beta/\nu = d = 2$ is nicely satisfied within statistical errors in both models.

Table 5.7: Results of the fit to the data of $|M_L|(\beta_c^{(1)})$ with the scaling law (5.8) on L^2 lattices with $L \geqslant L_{\min}$, for $N = 7$.

$N = 7$			
$L_{\min}$	A	β/ν	χ^2/d.o.f.
32	1.00653(48)	0.12210(08)	5.5
64	1.00858(70)	0.12243(12)	3.7
128	1.01074(94)	0.12277(15)	2.0
256	1.0146(16)	0.12336(26)	0.40
384	1.0162(22)	0.12359(34)	0.19
512	1.0177(38)	0.12381(56)	0.16
640	1.0185(57)	0.12393(84)	0.28

Table 5.8: Results of the fit to the data of $|M_L|(\beta_c^{(1)})$ with the scaling law (5.8) on L^2 lattices with $L \geqslant L_{\min}$, for $N = 17$.

$N = 17$			
$L_{\min}$	A	β/ν	χ^2/d.o.f.
32	1.00388(51)	0.12111(09)	7.98
64	1.00620(69)	0.12149(12)	3.58
128	1.0089(11)	0.12191(18)	1.54
256	1.0107(15)	0.12219(24)	0.74
384	1.0113(24)	0.12228(36)	1.36

We can cross-check our determination of the critical exponent η by an independent method, which does not rely on the prior knowledge of the critical coupling, but is based on the construction of a suitable universal quantity (22**?**). The idea is to plot $\chi_L^{(M_R)} L^{\eta-2}$ versus $B_4^{(M_R)}$ and to look for the value of η which optimizes the overlap of curves from different volumes. We found that, both in

Table 5.9: Results of the fit to the data of $\chi_L^{(M)}(\beta_c^{(1)})$ with the scaling law (5.9) on L^2 lattices with $L \geqslant L_{\min}$, for $N = 7$.

$N = 7$			
$L_{\min}$	B	γ/ν	χ^2/d.o.f.
32	0.00558(07)	1.7402(23)	2.38
64	0.00540(09)	1.7457(29)	1.32
128	0.00522(12)	1.7508(38)	0.68
256	0.00518(20)	1.7520(61)	0.84
384	0.00546(33)	1.7443(93)	0.70
512	0.00489(52)	1.760(16)	0.28
640	0.00444(76)	1.775(25)	0.0066

$Z(7)$ and $Z(17)$, $\eta = 1/4$ is this optimal value, since it gives the best overlap of these curves in the region of values corresponding to the first phase transition, *i.e.* the lower branch of the curves of Fig. **??**. This result for η agrees with the determinations $\eta = 2 - \gamma/\nu$ from the FSS analysis.

As for the second critical coupling $\beta_c^{(2)}$, we used the same method adopted for $\beta_c^{(1)}$, but applied now to $B_4^{(M_R)}$ and m_ψ. Our best estimates are

$$N = 7: \quad \beta_c^{(2)} = 1.8775(75)\ , \qquad\qquad N = 17: \quad \beta_c^{(2)} = 10.13(12)\ .$$

The standard FSS analysis applied to the susceptibility $\chi_L^{(M_R)}$ of the rotated magnetization M_R at $\beta_c^{(2)}$ leads to the result for the critical indices γ/ν given in Tables 5.11 and 5.12 [1].

Also in this case the critical index η can be determined by an independent method, irrespectively of the knowledge of $\beta_c^{(2)}$: $M_R L^{\eta/2}$ is plotted versus m_ψ and the value of η is searched for, which optimizes the overlap of data points coming from different volumes. The results we found for η in $Z(7)$ and $Z(17)$ are in perfect agreement with the theoretical prediction $\eta^{(2)} = 4/N^2$ (see Fig. **??**).

We studied also the specific heat at the two transitions, finding that, in contrast to the case of first- and second-order phase transitions, it does not reflect

[1] We do not report in this work the determinations of β/ν by the FSS analysis of the rotated magnetization M_R, since they are affected by large statistical and systematic uncertainties.

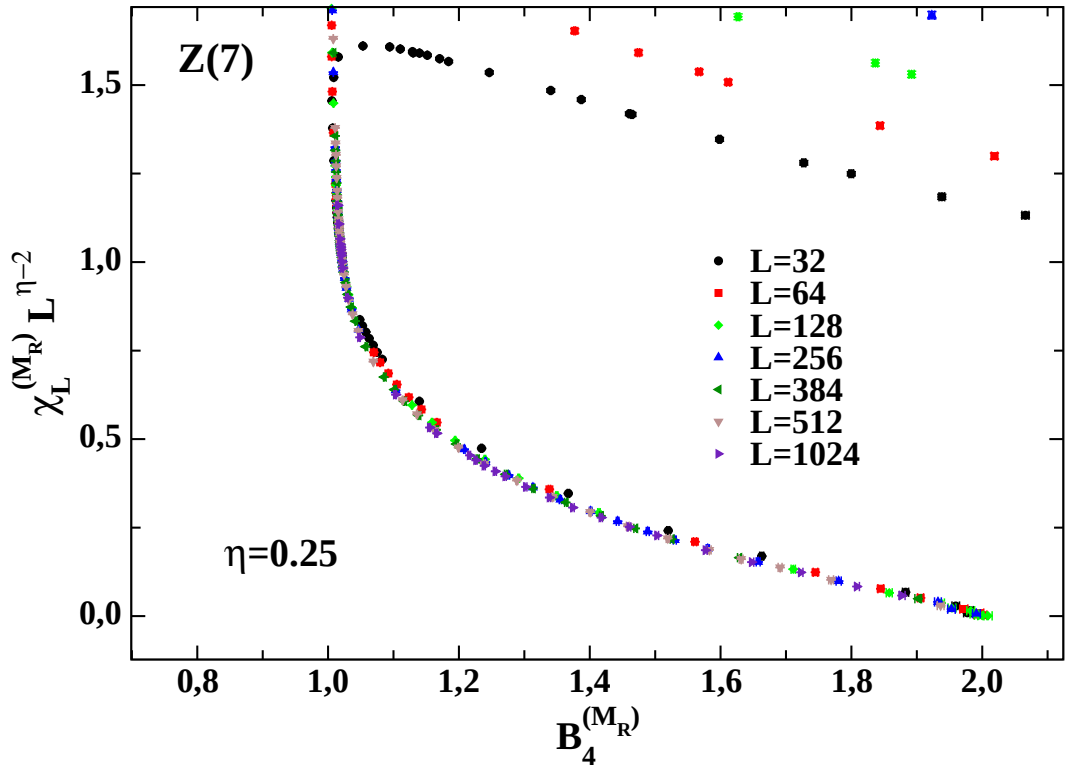

Figure 5.17: - Correlation between $\chi_L^{(M_R)} L^{\eta-2}$ and the Binder cumulant $B_4^{(M_R)}$ for $\eta = 0.25$ in $Z(7)$ on lattices with L ranging from 128 to 1024.

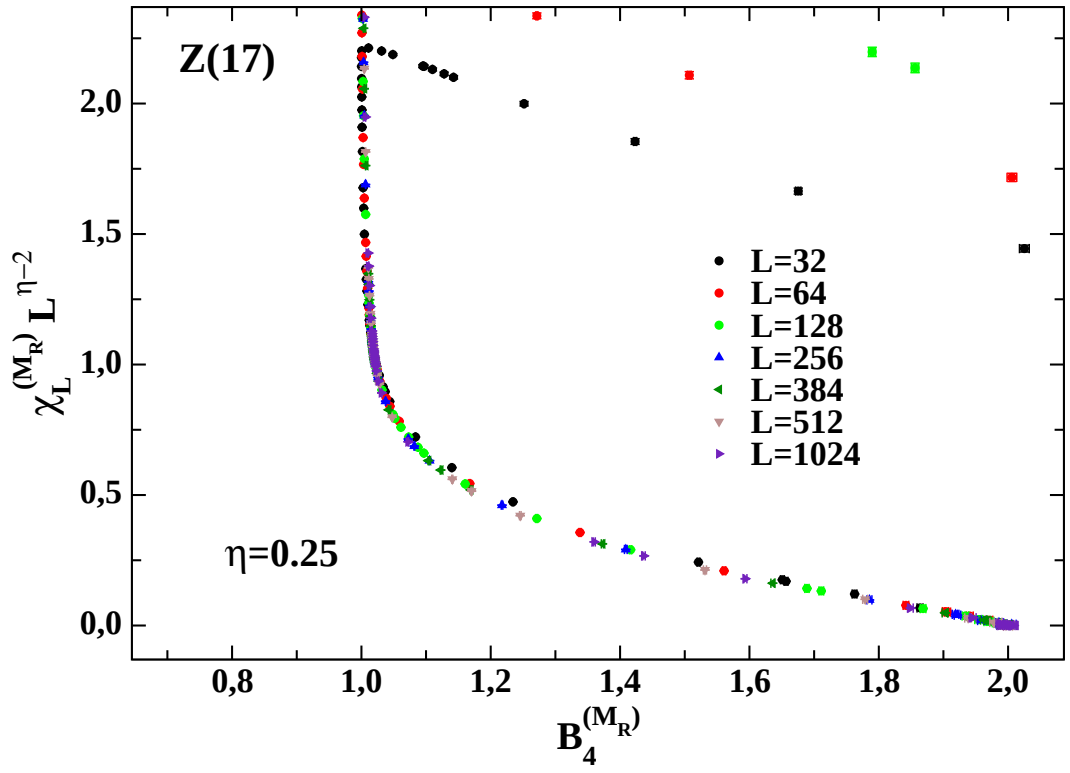

Figure 5.18: - Correlation between $\chi_L^{(M_R)} L^{\eta-2}$ and the Binder cumulant $B_4^{(M_R)}$ for $\eta = 0.25$ in $Z(17)$ on lattices with L ranging from 128 to 1024.

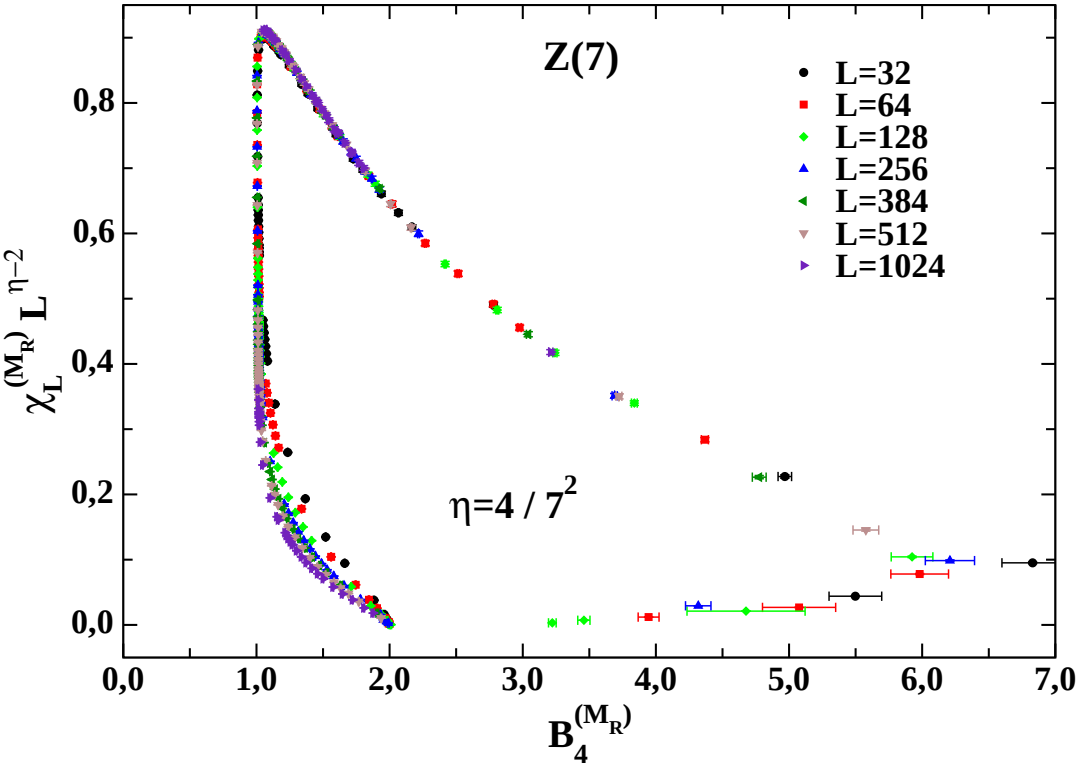

Figure 5.19: - Correlation between $\chi_L^{(M_R)} L^{\eta-2}$ and the Binder cumulant $B_4^{(M_R)}$ for $\eta = 4/N_2$ in $Z(7)$ on lattices with L ranging from 128 to 1024.

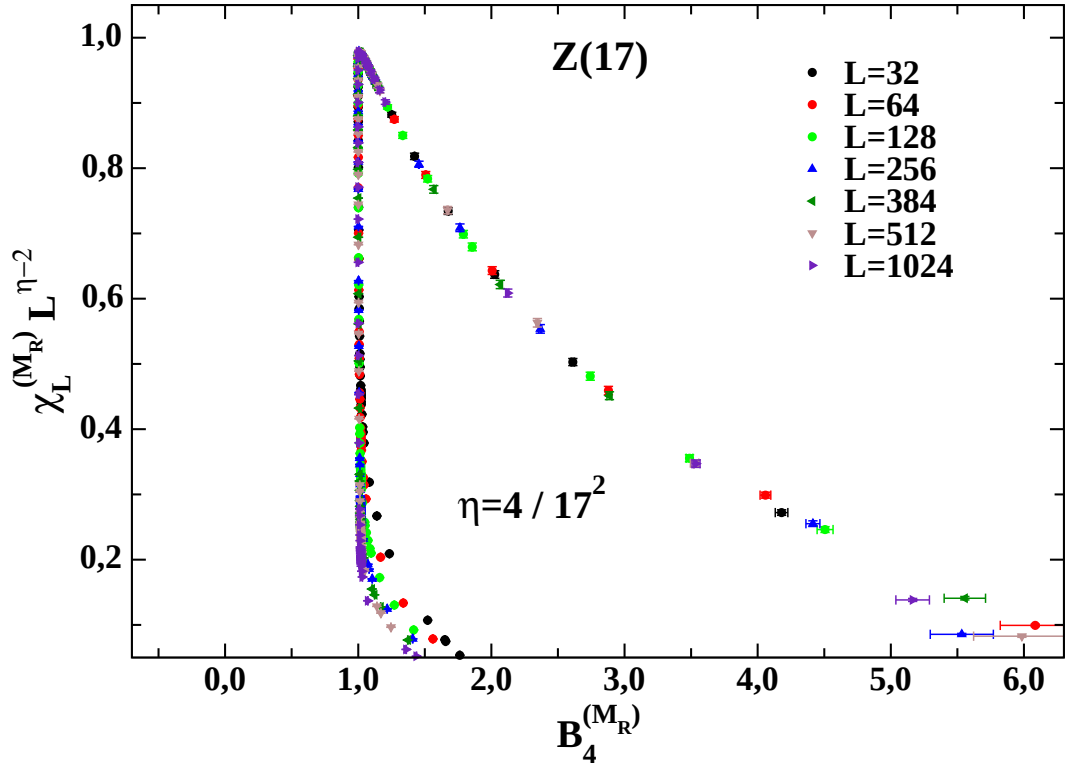

Figure 5.20: - Correlation between $\chi_L^{(M_R)} L^{\eta-2}$ and the Binder cumulant $B_4^{(M_R)}$ for $\eta = 4/N^2$ in $Z(17)$ on lattices with L ranging from 128 to 1024.

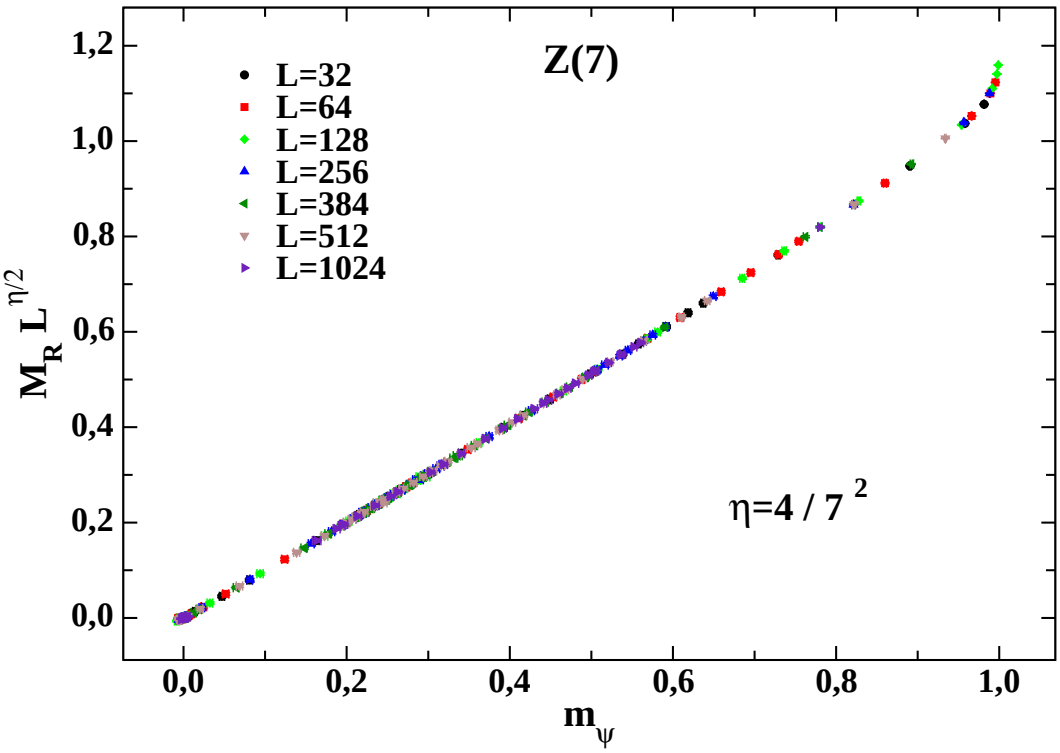

Figure 5.21: - Correlation between $M_R L^{\eta/2}$ and m_ψ for $\eta = 4/7^2$ in $Z(7)$ on lattices with L ranging from 128 to 1024.

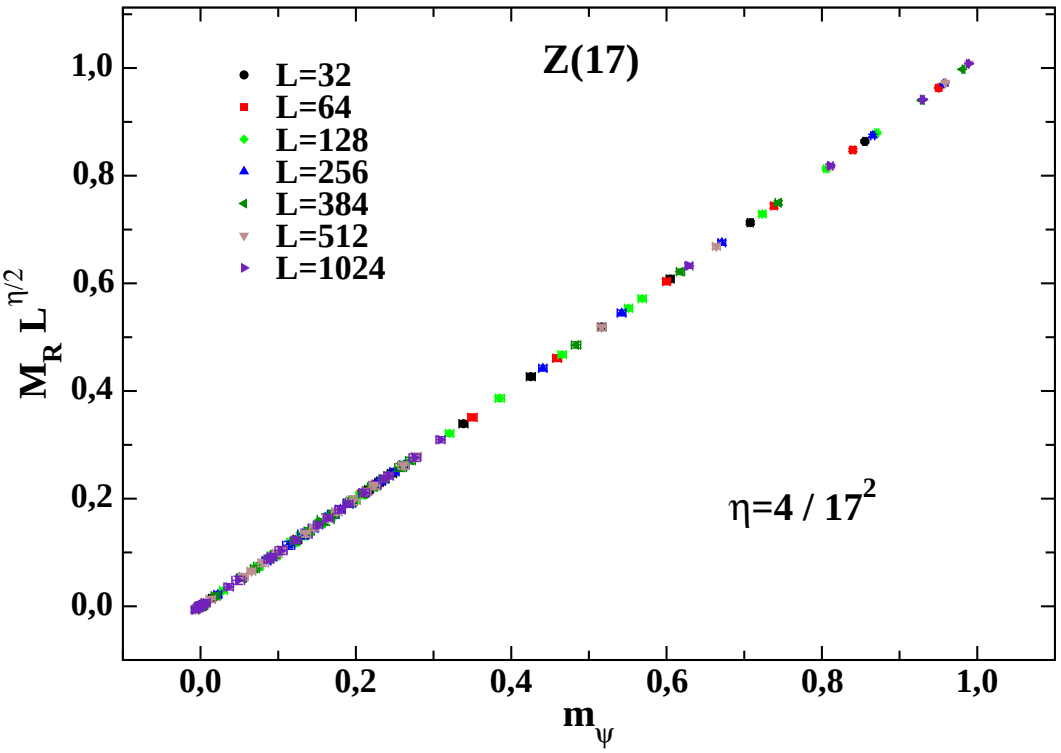

Figure 5.22: - Correlation between $M_R L^{\eta/2}$ and m_ψ for $\eta = 4/17^2$ in $Z(17)$ on lattices with L ranging from 128 to 1024.

Table 5.10: Results of the fit to the data of $\chi_L^{(M)}(\beta_c^{(1)})$ with the scaling law (5.9) on L^2 lattices with $L \geqslant L_{\min}$, for $N = 17$.

$N = 17$			
$L_{\min}$	B	γ/ν	χ^2/d.o.f.
32	0.00559(08)	1.7372(26)	2.7
64	0.00532(11)	1.7453(35)	0.39
128	0.00521(15)	1.7484(46)	0.16
256	0.00514(23)	1.7507(71)	0.15
384	0.00522(31)	1.7483(92)	0.13

any nonanalytical critical properties at the critical temperatures, thus confirming that only BKT transitions are at work here (see Figs. 5.23 and 5.24). For completeness I want to show you also the Binder cumulant of the energy derived from 3.7 only for the case of $Z(5)$ model (see Fig. 5.25). Clearly you can see the absence of any minima for the whole range of the critical coupling signaling that no first-order phase transitions are at work here.

5.4 Behavior of the helicity modulus

We use the following definition to evaluate the *helicity modulus* (31, 32)

$$\Upsilon = \langle e \rangle - L^2 \beta \left\langle s^2 \right\rangle , \tag{5.10}$$

where

$$e \equiv \frac{1}{L^2} \sum_{<ij>_x} \cos\left(\theta_i - \theta_j\right) \qquad and \qquad s \equiv \frac{1}{L^2} \sum_{<ij>_x} \sin(\theta_i - \theta_j)$$

and the notation $< ij >_x$ means nearest-neighbors spins in the x-direction.

Finally, in Figs. 5.26, 5.27 and 5.28 we present the behavior with β of the helicity modulus (5.10). This quantity is constructed in such a way that it should exhibit a discontinuous jump (in the thermodynamic limit) at the critical temperature separating the disordered phase from the massless one, if the transition

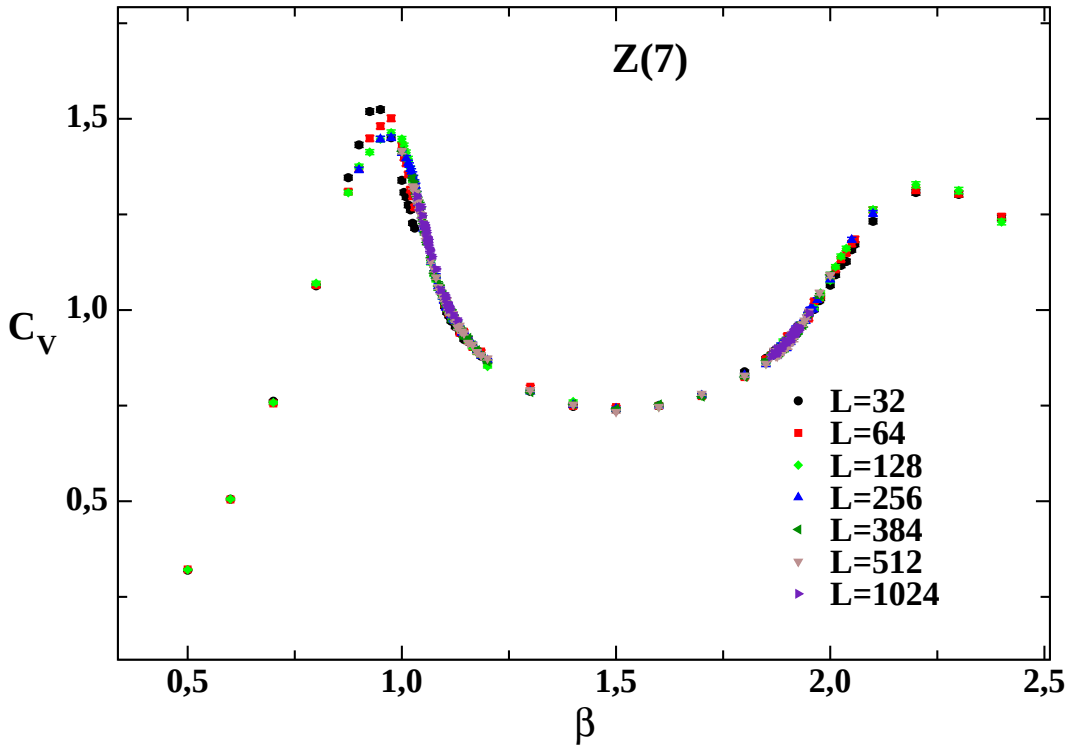

Figure 5.23: - Specific heat for $Z(7)$ on different lattices sizes.

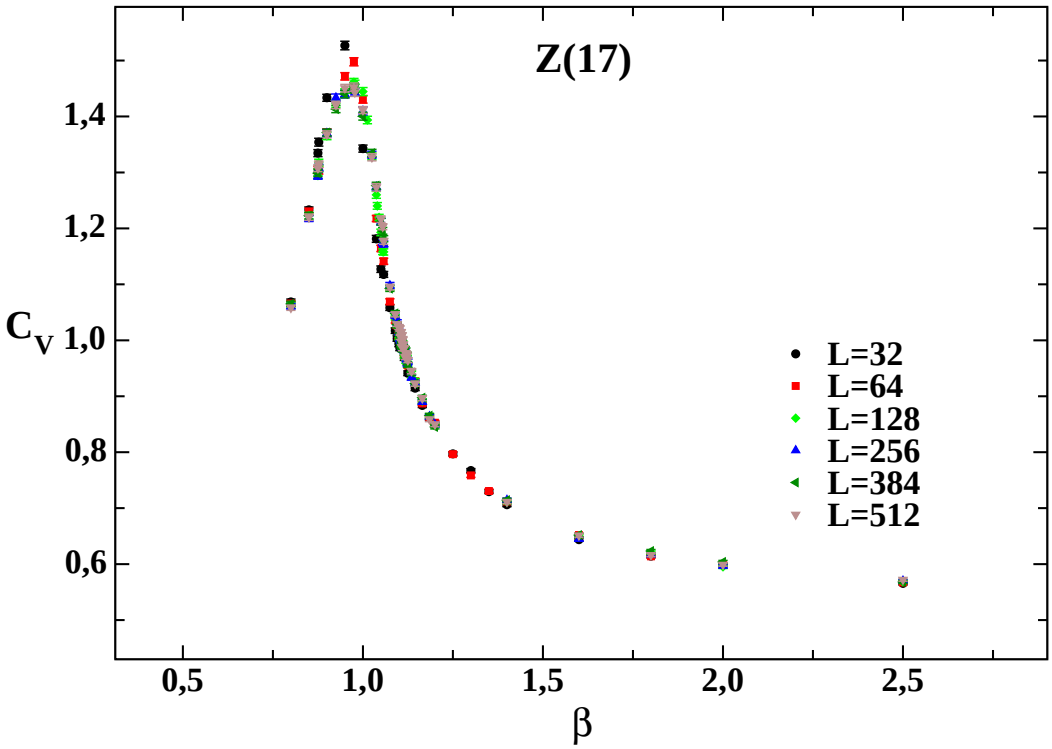

Figure 5.24: - Specific heat for $Z(17)$ on different lattices sizes. For simplicity we show only the behavior in the region of the transition from disordered to massless phase.

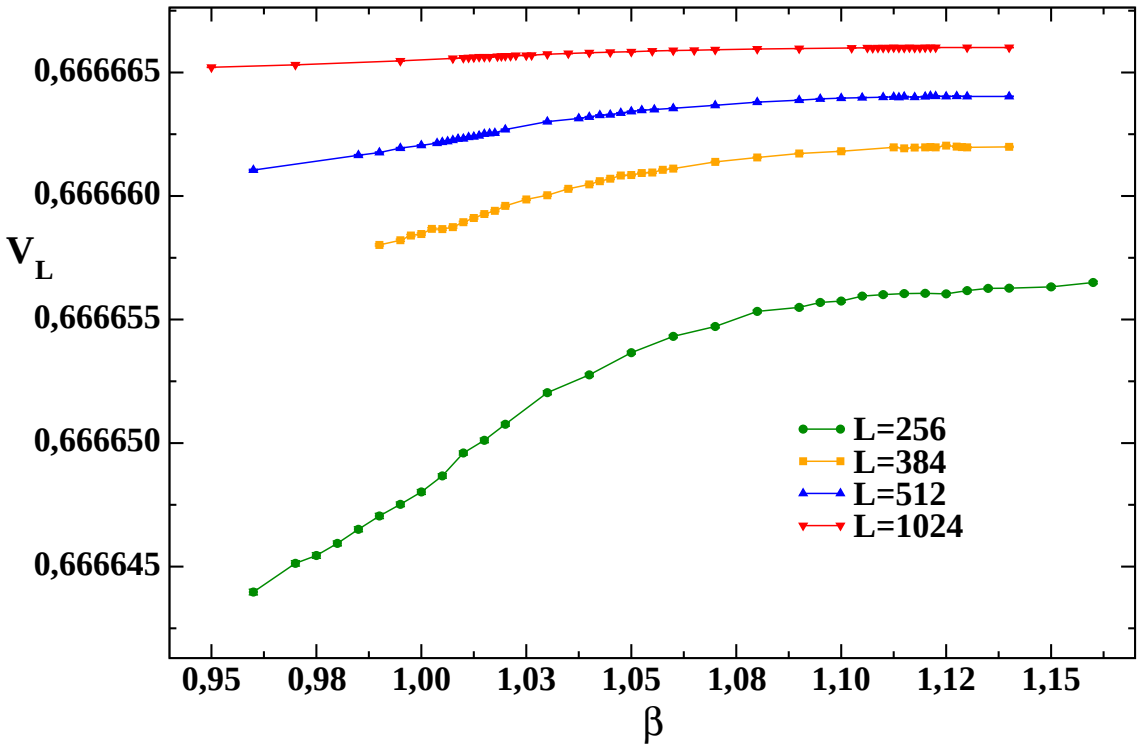

Figure 5.25: - Binder cumulant of the energy. The picture represent the case of the $Z(5)$ clock model.

Table 5.11: Results of the fit to the data of $\chi_L^{(M_R)}(\beta_c^{(2)})$ with the scaling law (5.9) on L^2 lattices with $L \geqslant L_{min}$, for $N = 7$.

$N = 7$			
L_{min}	A	γ/ν	χ^2/d.o.f.
32	0.8767(37)	1.92340(71)	2.02
64	0.8833(47)	1.92219(87)	1.41
128	0.8858(57)	1.9217(11)	1.57
256	0.8997(93)	1.9193(16)	1.02
384	0.916(15)	1.9166(25)	0.68
512	0.921(24)	1.9158(39)	0.98
640	0.942(34)	1.9124(54)	1.07

is of infinite order (BKT). Since the Kosterlitz-Thouless RG equations for the XY model (1, 2, 3, 33, 34) leads to the prediction that the helicity modulus Υ jumps from the value $2/(\pi\beta)$ to zero at the critical temperature, one can check if the same occurs for vector Potts models. In Figs. 5.26, 5.27 and 5.28 we plot a red line, representing the function $2/(\pi\beta)$; the crossing between this line and the curves formed by data points of Υ approaches indeed $\beta_c^{(1)}$ when the lattice size increases.

The knowledge of the behavior with β of the helicity modulus provides us with another method for the determination of the critical index η following the relation 3.11, which allows us to get the value of η at any fixed β in the BKT phase, if the value of Υ at that β is known.

A simple inspection of the behavior of Υ with β, shown in Figs. 5.26, 5.27 and 5.28, tells us that, for a given N, η in the BKT phase decreases monotonically from a value compatible with $\eta^{(1)} = 1/4$, taken at the first critical coupling $\beta_c^{(1)}$, to a value compatible with $\eta^{(2)} = 4/N^2$, taken at the second critical coupling. In some sense, the N^2 drop of the value of η at the second transition is related to increasing distance between $\beta_c^{(2)}$ and $\beta_c^{(1)}$. According to 3.11, the discontinuous jump of Υ to zero in the thermodynamic limit when β becomes smaller than $\beta_c^{(1)}$, *i.e.* when the disordered phase is entered, implies the sudden jump to infinity of η. This is consistent with the fact that the spin-spin correlator in

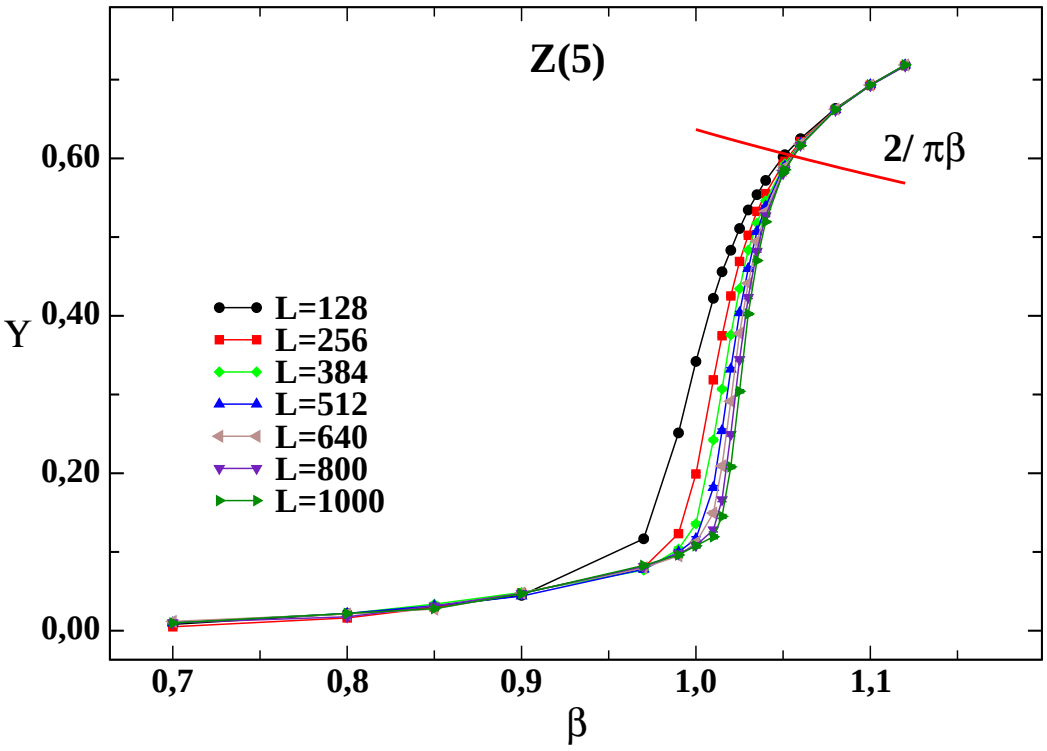

Figure 5.26: - Helicity modulus versus β in $Z(5)$ on lattices with various sizes.

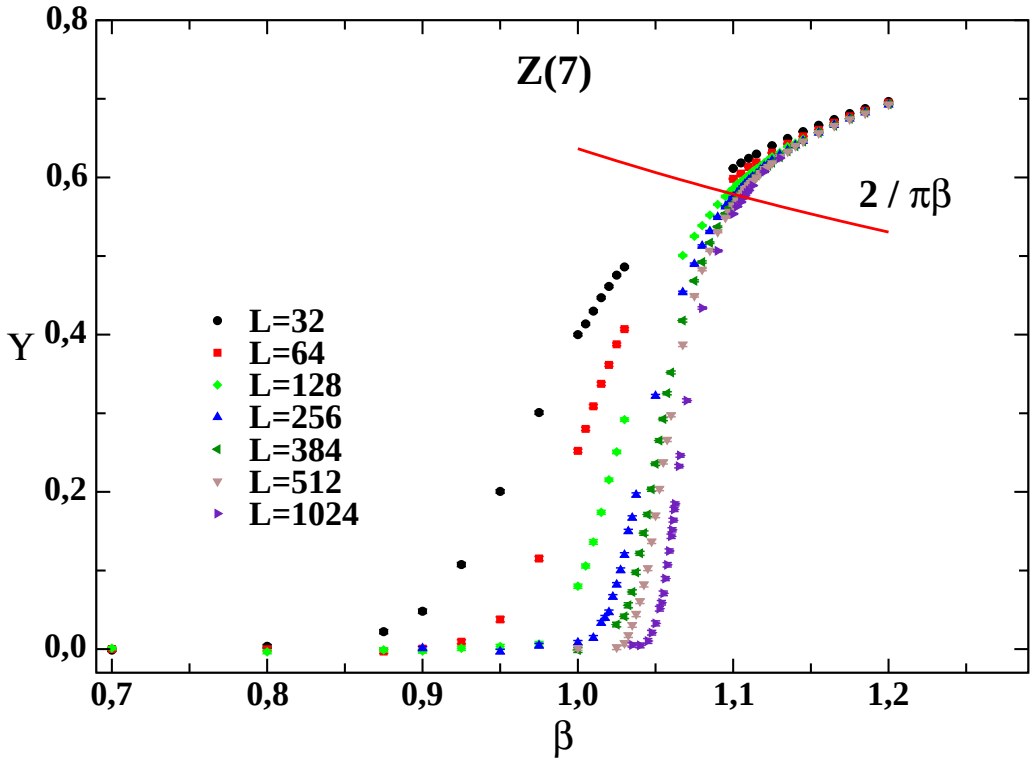

Figure 5.27: - Helicity modulus versus β in $Z(7)$ on lattices with various sizes.

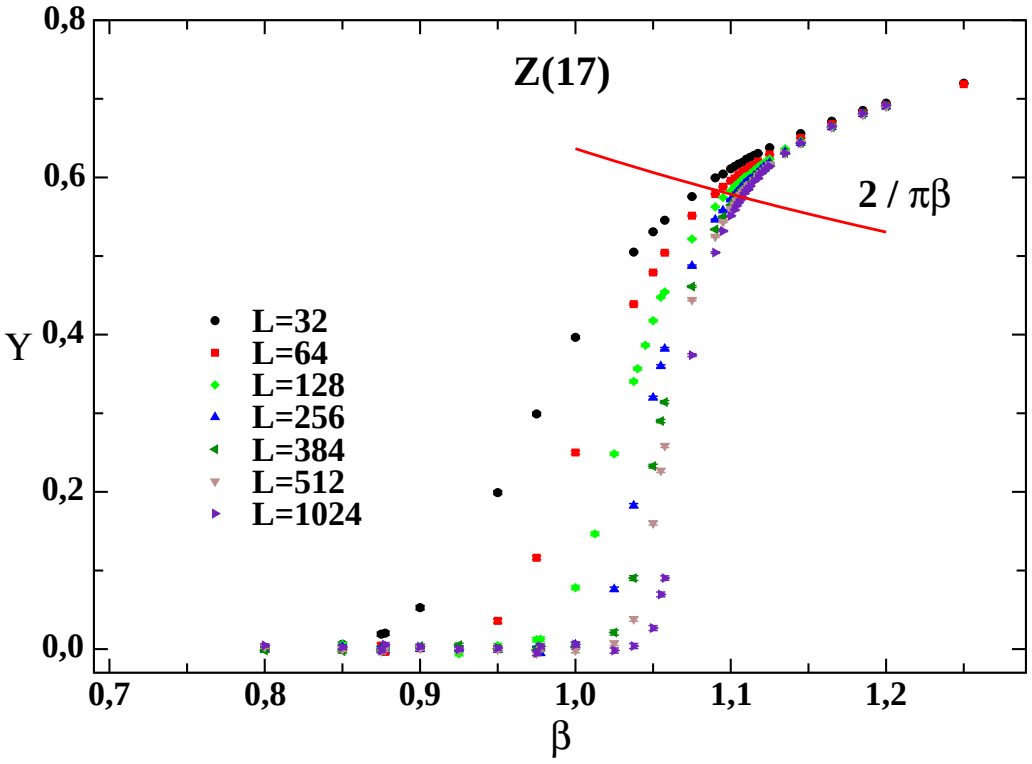

Figure 5.28: - Helicity modulus versus β in $Z(17)$ on lattices with various sizes.

Table 5.12: Results of the fit to the data of $\chi_L^{(M_R)}(\beta_c^{(2)})$ with the scaling law (5.9) on L^2 lattices with $L \geqslant L_{min}$, for $N = 17$.

$N = 17$			
L_{min}	B	γ/ν	χ^2/d.o.f.
32	0.9319(47)	1.98933(89)	1.65
64	0.9408(68)	1.9878(12)	1.38
128	0.9533(89)	1.9857(16)	0.67
256	0.954(16)	1.9856(27)	0.83
384	0.950(24)	1.9861(40)	1.09
512	0.931(38)	1.9892(62)	1.44
640	0.911(59)	1.9925(98)	2.67

the disordered phase decays exponentially with the distance and that this can be mimicked only by a power-like decay with an infinite η. In this respect, the slower approach to zero of Υ in $Z(5)$ for β smaller than $\beta_c^{(1)}$ suggests that the disordered phase of this model is characterized by a correlation length much larger than the lattice sizes considered so far. The η behavior coming from Υ is shown in Figs. 5.29, 5.30 and 5.31. The horizontal red line represent the predicted η value for the transition from disordered to massless phase while the vertical line is the estimated critical temperature. The analysis of these intersection point gives a value for the $\beta_c = 1.056$ for the $Z(5)$ model, a little bit much larger than the previous evaluation. For the $Z(7)$ and $Z(17)$ the values of the critical temperatures are in good agreement with the last determinations.

5.4.1 Helicity modulus and the beta function

In this section I want to show the connection between the helicity modulus and the beta function in order to understand, or to try to understand if

- the beta function vanishes at the critical temperature, thus signalling that the intermediate phase is of BKT-type;
- the value of the index ν that governing the behavior of the correlation length (2.1) is equal to 1/2 as predicted by theoretical studies.

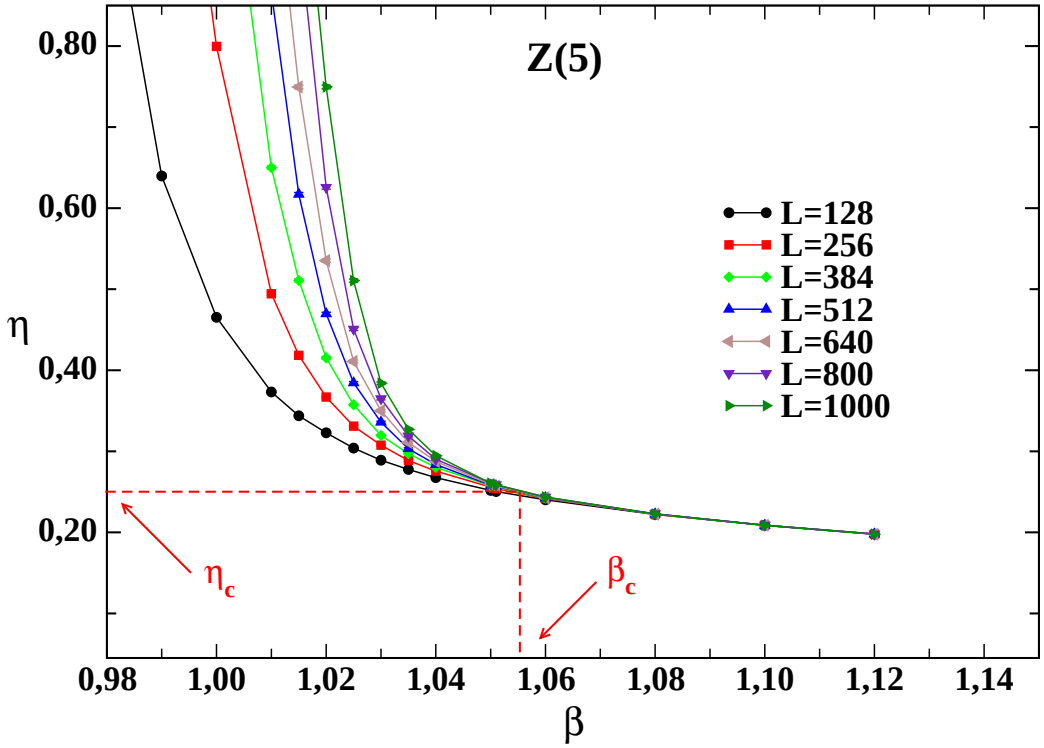

Figure 5.29: - Magnetic critical exponent η derived from equation (3.11) for $Z(5)$.

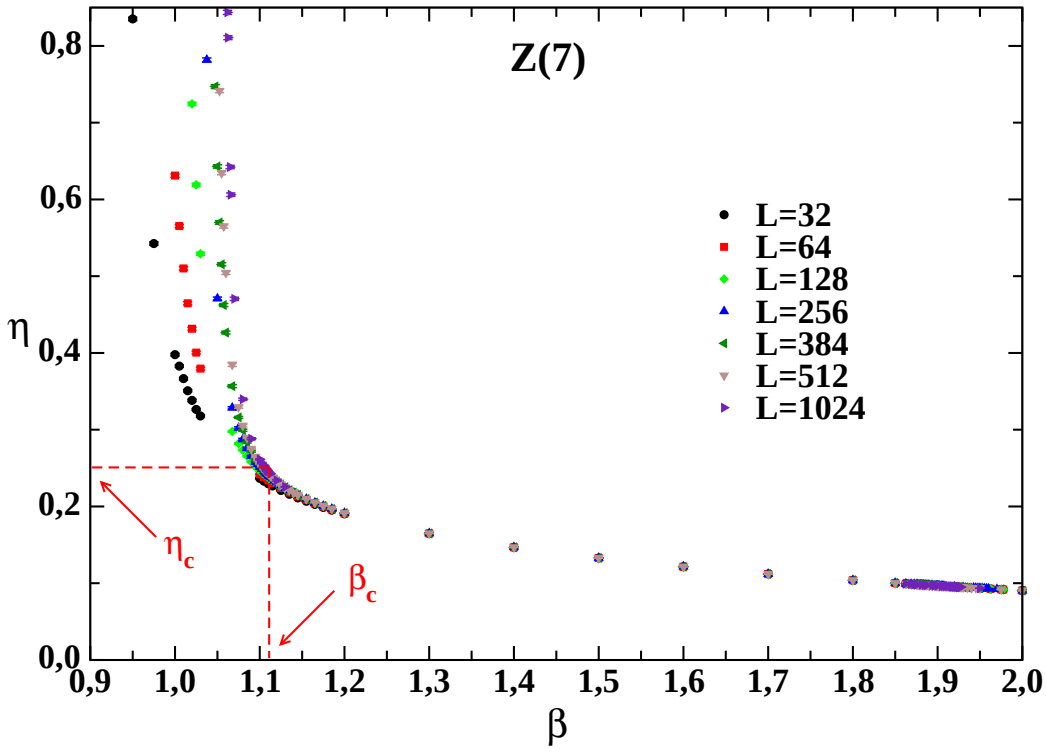

Figure 5.30: - Magnetic critical exponent η derived from equation (3.11) for $Z(7)$.

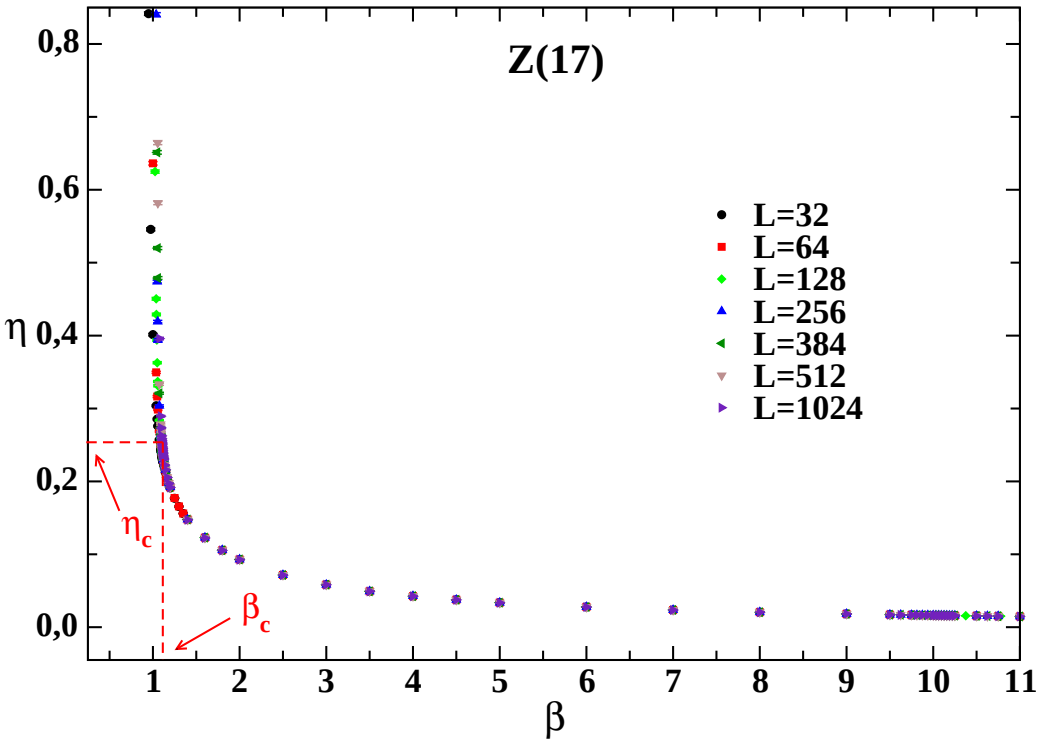

Figure 5.31: - Magnetic critical exponent η derived from equation (3.11) for $Z(17)$.

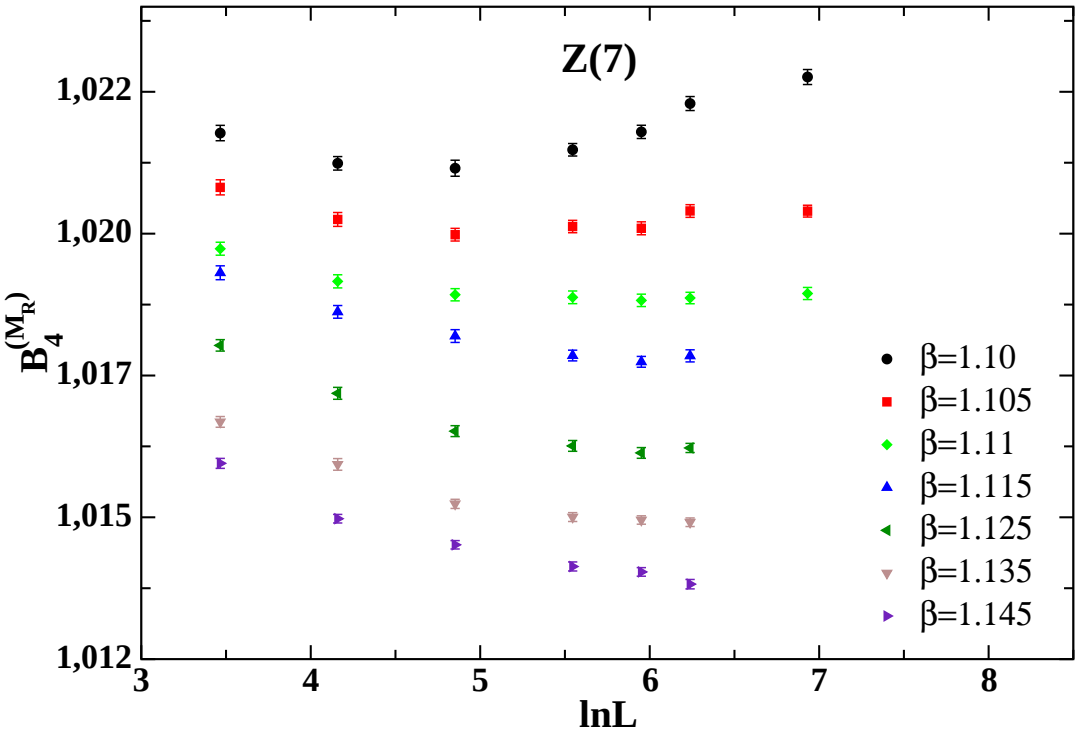

Figure 5.32: - $B_4^{(M_R)}$ as a function of $ln(L)$ over $32 \leqslant L \leqslant 1024$, for various temperature near criticality. $B_4^{(M_R)}$ is L independent, within a small statistical error, over $128 \leqslant L \leqslant 1024$ and $256 \leqslant L \leqslant 512$ for $\beta = 1.11$ and 1.115 respectively. The case considered is the $Z(7)$ model.

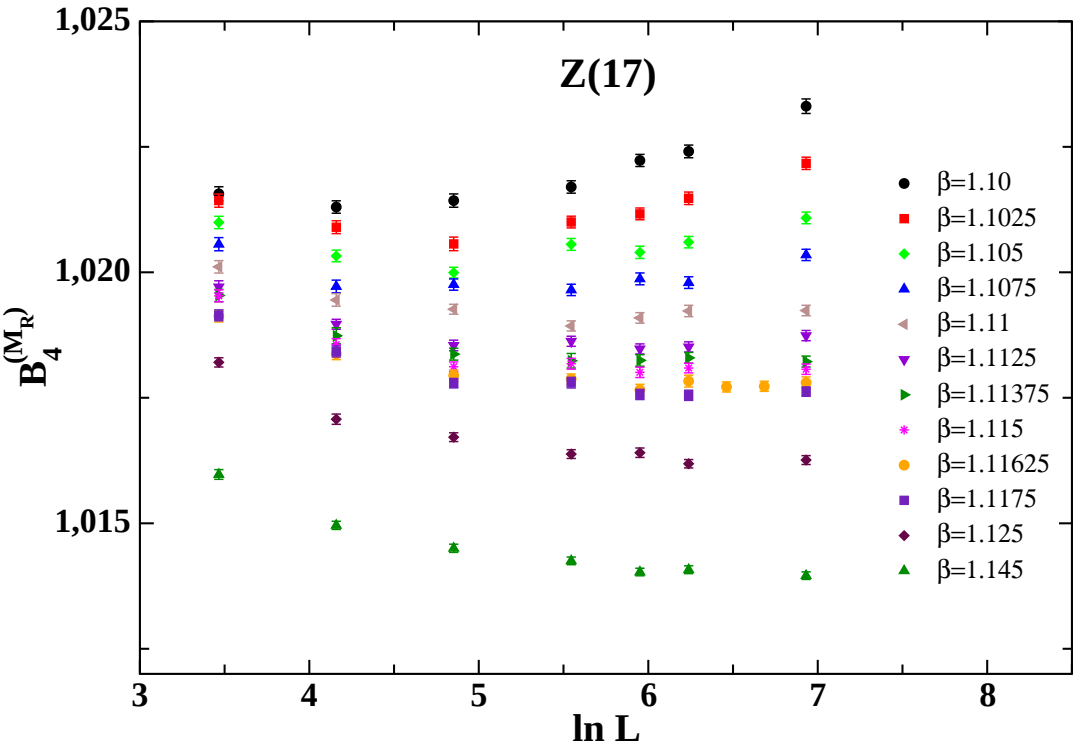

Figure 5.33: - $B_4^{(M_R)}$ as a function of $ln(L)$ over $32 \leqslant L \leqslant 1024$, for various temperature near criticality. $B_4^{(M_R)}$ display a L-independence, over a larger range of lattice sizes for $1.1125 \leqslant \beta \leqslant 1.11375$. The case considered is the $Z(17)$ model.

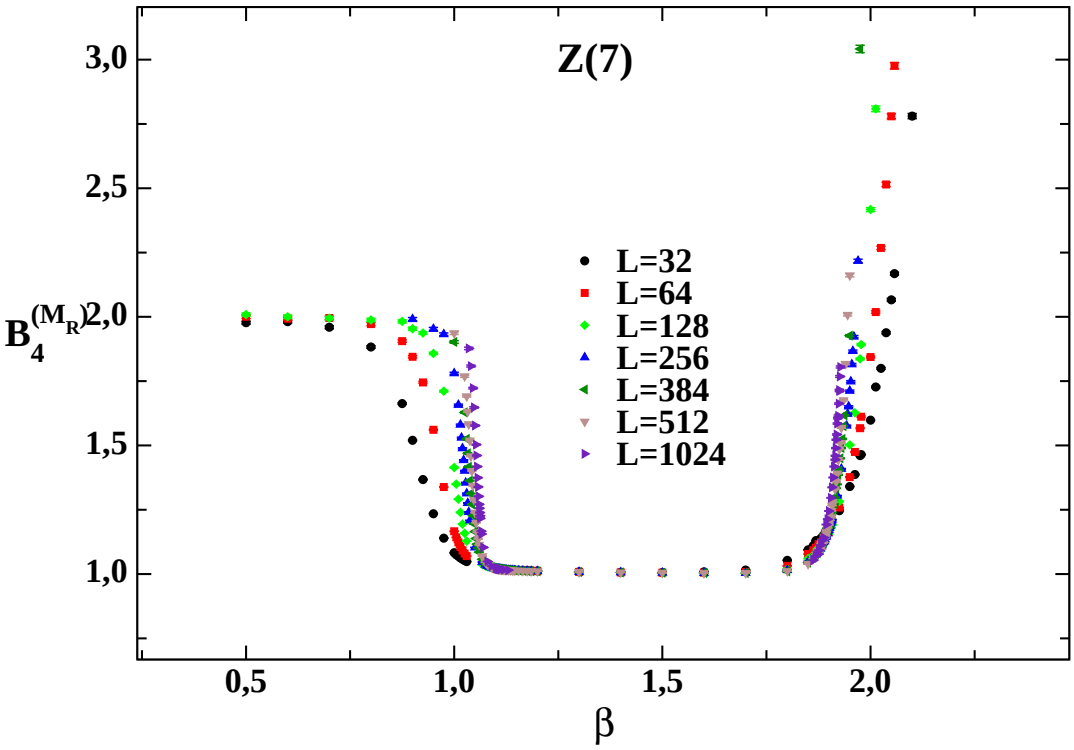

Figure 5.34: - Binder cumulant $B_4^{(M_R)}$ for the $2D$ $Z(7)$ vector model on different lattices sizes.

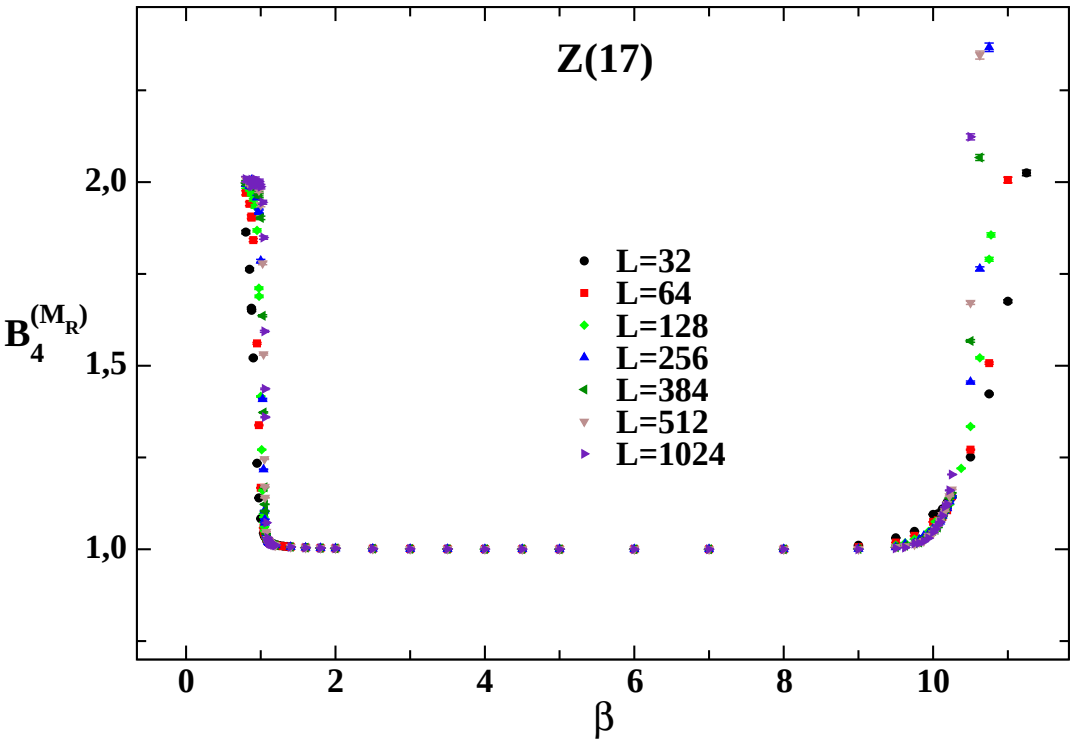

Figure 5.35: - Binder cumulant $B_4^{(M_R)}$ for the $2D$ $Z(17)$ vector model on different lattices sizes.

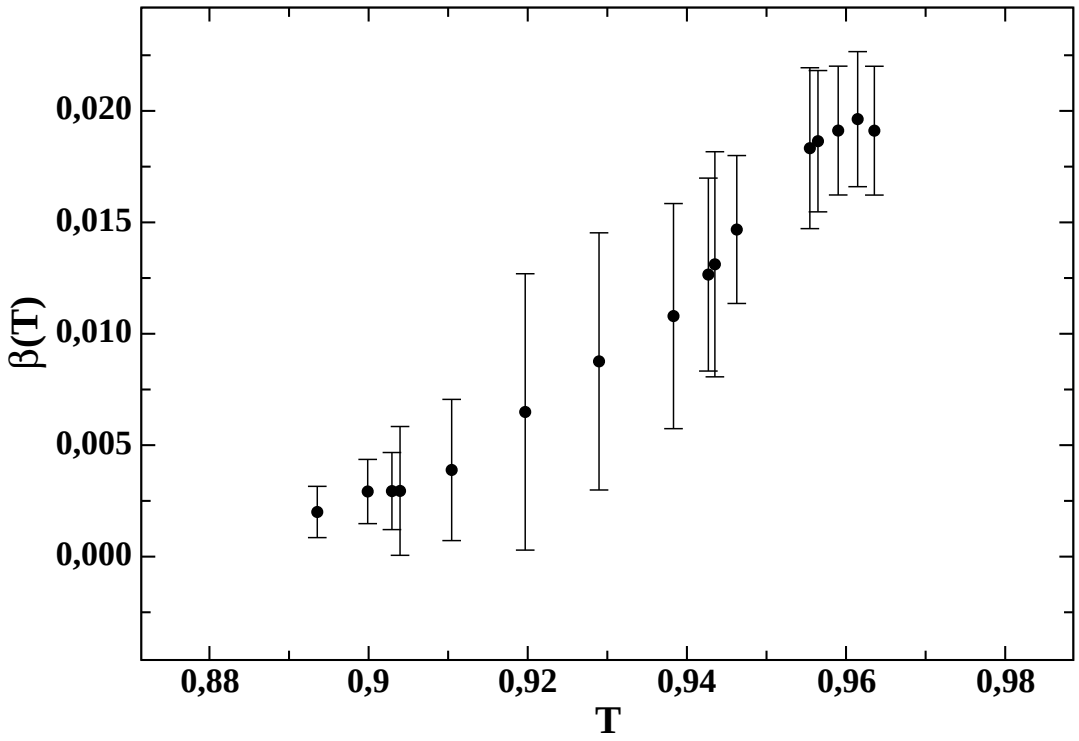

Figure 5.36: - The beta function obtained for the 512×512 and 1024×1024 lattices evaluated for the $2D$ $Z(7)$ vector model.

Since we expect that $2D$ $Z(5,7,17)$ clock models is in the same universality class of the $2D$ XY model, the helicity modulus $\Upsilon(L,T)/J$ (where $T = 1/\beta$) for the last model is dimensionless, thus, should be keep constant under scaling transformations. Namely, the beta function can be obtained by defining a function $T = F(L)$ such that $\Upsilon(L^{'}, F(L^{'})) = \Upsilon(L, F(L)) = \Upsilon_p$ ia a constant, a physical value of the helicity modulus. The beta function is defined as:

$$\beta(T) = -\lim_{L\to\infty} \frac{dT}{dln(L)} \tag{5.11}$$

For large enough L, where finite-size effects influencing the calculation of the beta-function are small, the Kosterlitz-Thouless theory suggests the following form of $\beta(T)$:

$$\beta(T > T_c) = c(T - T_c)^{1+\nu} \qquad\qquad \beta(T \leqslant T_c) = 0. \tag{5.12}$$

The beta-function can be determined as follows (37). For a pair of lattices L_1, L_2 let us consider the calculated $\Upsilon(L_1,T)$ and $\Upsilon(L_2,T)$ for all values of T. Choosing a value Υ for the helicity modulus we can determine two pairs (T_1, L_1) and (T_2, L_2) such that $\Upsilon = \Upsilon(L_1,T_1) = \Upsilon(L_2,T_2)$. Using these two points we calculate a value of the beta-function at $\bar{T} = (T_1 + T_2)/2$ as follows

$$\beta(\bar{T}) = -\frac{T_2 - T_1}{ln(L_2) - ln(L_1)}. \tag{5.13}$$

By choosing a different value of the helicity modulus we can obtain a new value for $\beta(\bar{T})$ at a different value $\bar{T}$. In Fig. 5.36 we can see how beta-function approaches the zero value in the region of the critical temperature (in this case $T_c \approx 0.8999$ for the $Z(7)$ vector model) for the pair $L_1 = 512$ and $L_2 = 1024$. I want to mention the fact that this determination is just qualitative and not so refined. We then fit the calculated $\beta(T)$ to the form given by Kosterlitz-Thouless expression (5.12). Using c, T and ν as fitting parameters we do not obtain a good stability for the fit since the error bars are very large. In conclusion, we cannot extract ν from the fit of the beta-function and, only setting $\nu = 1/2$ and the critical temperature estimated for the model considered here (the Z(7) model), we obtain a optimum stability for the parameter c together with a good $\chi^2/n.d.f.$.

6

Discussion

We have determined the two critical couplings of the $2D$ $Z(N = 5, 7, 17)$ vector models and given estimates of the critical indices η at both transitions. Our findings support for all $N \geq 5$ the standard scenario of three phases: a disordered phase at high temperatures, a massless or BKT one at intermediate temperatures and an ordered phase, occurring at lower and lower temperatures as N increases. This matches perfectly with the $N \to \infty$ limit, *i.e.* the $2D$ XY model, where the ordered phase is absent or, equivalently, appears at $\beta \to \infty$. Considering the determinations of the critical coupling $\beta_c^{(1,2)}(N)$ obtained in this work for $N = 5, 7$ and 17 (see Refs. (21), (22)) and those for $N = 6$, 8 and 12 of Ref. (11), one can verify that $\beta_c^{(1)}(N)$ approaches the $2D$ XY value, $\beta_c^{(1)} = 1.1199$, exponentially in N or even faster, while $\beta_c^{(2)}(N)$ grows to infinity with N^2.

We have also found that the values of the critical index η at the two transitions are compatible with the theoretical expectations.

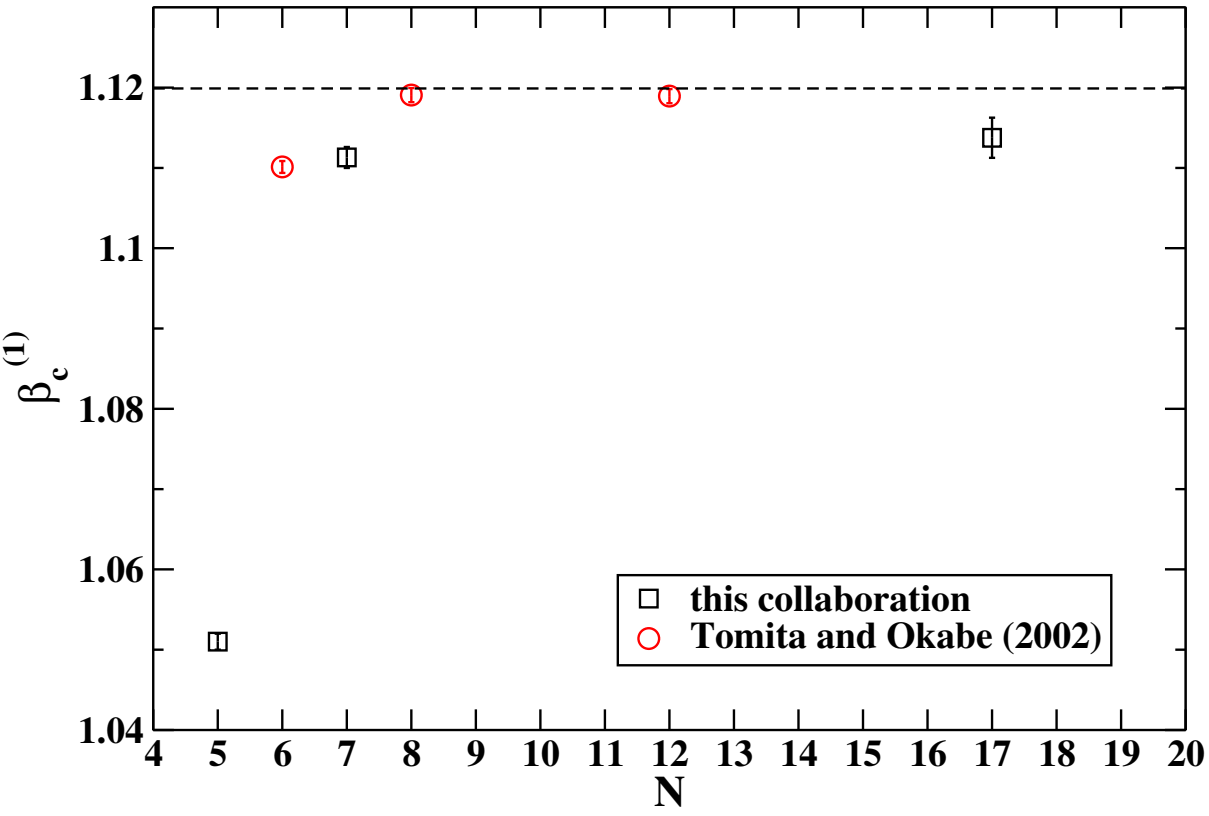

Figure 6.1: - Behavior with N of the known values of the critical coupling $\beta_c^{(1)}$ in $2D$ $Z(N)$ vector models. The horizontal dashed line represents the critical coupling of $2D$ XY, β_{XY}=1.1199, taken from Ref. (38).

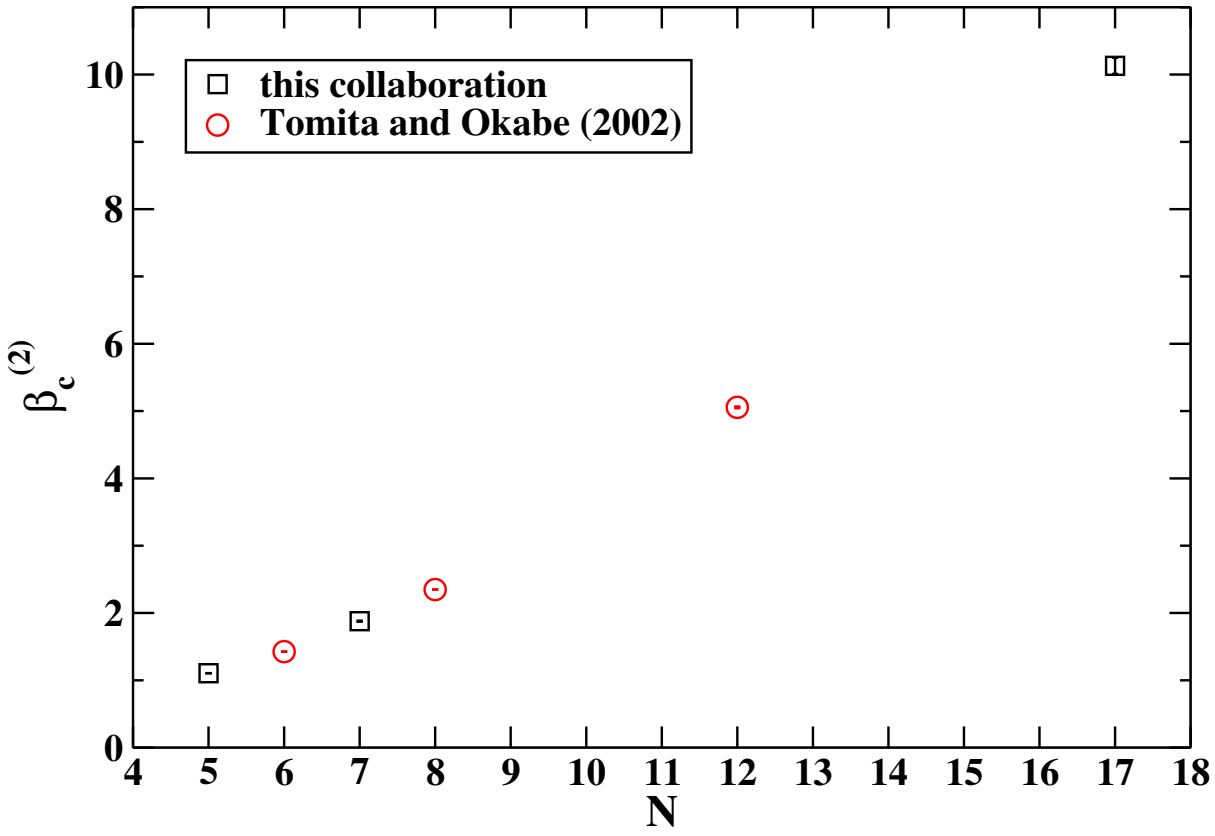

Figure 6.2: - Behavior with N of the known values of the critical coupling $\beta_c^{(2)}$ in $2D$ $Z(N)$ vector models.

Bibliography

[1] V. Berezinskii, Sov. Phys. JETP **32** (1971) 493. 1, 55

[2] J. Kosterlitz, D. Thouless, J. Phys. C **6** (1973) 1181. 1, 55

[3] J. Kosterlitz, J. Phys. C **7** (1974) 1046. 1, 5, 12, 55

[4] F. Y. Wu, Rev. Mod. Phys. **54** (1982) 235. 7

[5] S. Elitzur, R. B. Pearson, J. Shigemitsu, Phys. Rev. D **19** (1979) 3698. 2, 7, 32

[6] M. B. Einhorn, R. Savit, *A physical picture for the phase transitions in $Z(N)$-symmetric models*, Preprint UM HE 79-25. 7

[7] C. J. Hamer, J. B. Kogut, Phys. Rev. B **22** (1980) 3378. 7

[8] B. Nienhuis, J. Statist. Phys. **34** (1984) 731. 7

[9] L. P. Kadanoff, J. Phys. A **11** (1978) 1399. 7

[10] J. Fröhlich, T. Spencer, Commun. Math. Phys. **81** (1981) 527. 2, 7, 8

[11] Y. Tomita, Y. Okabe, Phys. Rev. B **65** (2002) 184405 [arXiv:cond-mat/0202161]. 2, 3, 8, 32, 69

[12] B. Svetitsky, L. Yaffe, Nucl. Phys B **210** (1982) 423. 2

[13] A. Ukawa, P. Windey, A. Guth, Phys. Rev. D **21** (1980) 1013. 2

[14] F. Y. Wu, J. Phys. C **12** (1979) L317. 2

[15] J. l. Cardy, J. Phys. A **13** (1980) 1507. 2

[16] E. Domany, D. Mukamel, A. Schwimmer, J. Phys. A **13** (1980) L311. 2

[17] P. Ruján, G. O. Williams, H. L. Frisch, G. Forgács, Phys. Rev. B **23** (1981) 1362; H. H. Roomany, H. W. Wyld, Phys. Rev. B **23** (1981) 1357. 2

[18] C. M. Lapilli, P. Pfeifer, C. Wexler, Phys. Rev. Lett. **96** (2006) 140603 [arXiv:cond-mat/0511559] 2

[19] S.K. Baek and P. Minnhagen, Phys. Rev. E **82** (2010) 031102 [arXiv:1009.0356 [cond-mat.stat-mech]]. 2, 3

[20] S.K. Baek, P. Minnhagen and B.J. Kim, Phys. Rev. E **80** (2009) 060101(R) (2009) [arXiv:0912.2830 [cond-mat.stat-mech]]. 2, 3, 10

[21] O. Borisenko, G. Cortese, R. Fiore, M. Gravina, A. Papa, *Critical properties of the two-dimensional Z(5) vector model*, PoS **LATTICE2010** (2010) 274. 69

[22] O. Borisenko, G. Cortese, R. Fiore, M. Gravina, A. Papa, Phys. Rev. **E83** (2011) 041120 [arXiv:1011.5806]. 43, 69

[23] M. S. S. Challa, D. P. Landau and K. Binder, Phys. Rev. B **34** (1986) 1841. 12, 35

[24] O. Borisenko, M. Gravina, A. Papa, J. Stat. Mech. **2008** (2008) P08009 [arXiv:0806.2081 [hep-lat]]. 22, 28, 29

[25] O. Borisenko, R. Fiore, M. Gravina, A. Papa, J. Stat. Mech. **2010** (2010) P04015 [arXiv:1001.4979 [hep-lat]]. 22

[26] R. Kenna and A. C. Irving, Nucl. Phys. B **485** (1997) 583 [arXiv:hep-lat/9601029]. 29

[27] M. Hasenbusch, J. Phys. A **38** (2005) 5869 [arXiv:cond-mat/0502556v2 [cond-mat.stat-mech]]. 29

[28] D. Loison, J. Phys.: Condens. Matter **11** (1999) L401. 35

[29] M. E. Fisher, M. N. Barber, D. Jasnow, Phys. Rev. A **8** (1973) 1111. 13

[30] O. Borisenko, G. Cortese, R. Fiore, M. Gravina, A. Papa, PoS **LATTICE2011** (2011) 304 [arXiv:1110.6385 [hep-lat]].

[31] P. Minnhagen, B.J. Kim, Phys. Rev. **B67** (2003) 172509. 51

[32] M. Hasenbusch, J. Stat. Mech. (2008) **P08003**. 51

[33] T. Ohta and D. Jasnow, Phys. Rev. **B20** (1979) 139. 55

[34] D.R. Nelson and J.M. Kosterlitz, Phys. Rev. Lett. **39** (1977) 1201. 13, 55

[35] J.E. van Himbergen, J. Phys. **C17** (1984) 5039. 13

[36] A. Yamagata and I. Ono, J. Phys. **A24** (1991) 265. 13

[37] P. Harten and P. Suranyi, Nucl. Phys. **B265** [FS15] 615 (1989); E. Manousakis, Rev. Mod. Phys. **63**, 1 (1991); 68
N. Schultka, E. Manousakis, arXiv:cond-mat/9310034.

[38] M. Hasenbusch, J. Phys. A **38** (2005) 5869 [arXiv:cond-mat/0502556]. 70